Journal of Crystal Growth 32 (1976) 335–349
© North-Holland Publishing Company

FILAMENTOUS GROWTH OF CARBON THROUGH BENZENE DECOMPOSITION

A. OBERLIN and M. ENDO *
Laboratoire Marcel Mathieu, Faculté des Sciences, CNRS, ER 131, 45045 Orléans-La-Source, France

and

T. KOYAMA
Shinshu University, Faculty of Engineering, 500 Wakasato Nagano City, Japan

Received 19 September 1975

Carbon fibres have been prepared by pyrolysing a mixture of benzene and hydrogen at about 1100°C. They have been studied by high resolution electron microscopy. These fibres have various external shapes and contain a hollow tube with a diameter ranging from 20 to more than 500 Å along the fibre axis. They consist of turbostratic stacks of carbon layers, parallel to the fibre axis, and arranged in concentric sheets like the "annual ring structure of a tree". These fibres have two textures resulting from different growth processes; core regions, made of long, straight and parallel carbon layers, are primarily formed by catalytic effect; the external regions correspond to a pyrolytic deposit occurring during the secondary thickening growth process. Very small cementite crystals, typically about 100 Å in diameter, have been identified by dark-field techniques at the tip of the central tube of each fibre. A model of fibre growth related to a surface diffusion of carbon species on the catalyst particle has been established.

1. Introduction

Filamentous growth of carbon has been studied by many authors [1–7]. The fibres grow from various substrates heat-treated from 250°C to 2500°C in atmospheres containing either carbon monoxide or hydrocarbon gases. Some low temperature forms (below 1500°C) often are improperly called whiskers because they are not crystallized and have no epitaxial relation with the substrate from which they grow. Some of these filaments have been found to be hollow tubes with the carbon layers parallel to the fibre axis and more or less bent cylindrically so that their *c* axis should be perpendicular to the filament axis.

One of the authors [8,9] has reported that a great number of carbon fibres were obtained by pyrolysing a mixture of benzene and hydrogen at about 1100°C. The fibre lengths were up to 25 cm and their diameters less than several hundred micrometres. The SEM studies have shown that these fibres consist of concentric sheets of carbon, set around the fibre axis, as the annual rings of a tree. Also, like in a tree the fibres may be divided into two or more branches. Evidence has been given in another paper [10] that the growth process begins with the formation of thin filaments (primary process) which are progressively thickened by a secondary processing consisting in a deposit of carbon on the primary filament. In this pyrolytic thickening process the diameter increases as pyrolysing temperature and time increase. However, it is impossible to obtain the two stages separately because they are statistically concomitant, though successive for a given part of the fibre. It has also been shown [11] that the final fibres are graphitizable when heat-treated up to 2900°C.

The present paper mainly deals with the texture both of the primary filaments and of the subsequent deposit, which have been studied by high resolution electron microscopy (using a Philips EM 300). In order to decrease the thickness of the fibres the concentration of benzene was lowered and the growing time

* Permanent address. Shinshu University, Faculty of Engineering, 500 Wakasato Nagano City, Japan.

shortened, so that the diameters of the fibres have been restricted to less than 8000 Å; then most of them are thin enough for TEM studies. The fibres thus were either directly deposited on grids covered with a thin supporting carbon film or transversally thin sectioned by ultra-microtomy. Combined techniques were used such as selected area electron diffraction (SAD), bright- and dark-field especially developed in our laboratory [12,13] as well as lattice-imaging [14].

2. Experimental

2.1. Main part of the fibres

The external shape of the fibres greatly varies as shown in fig. 1. Many of them are bead-like, each bead being spindle-shaped, others are cylindrical with or without more or less constricted regions. All of them contain a tube running parallel to the axis (see arrows

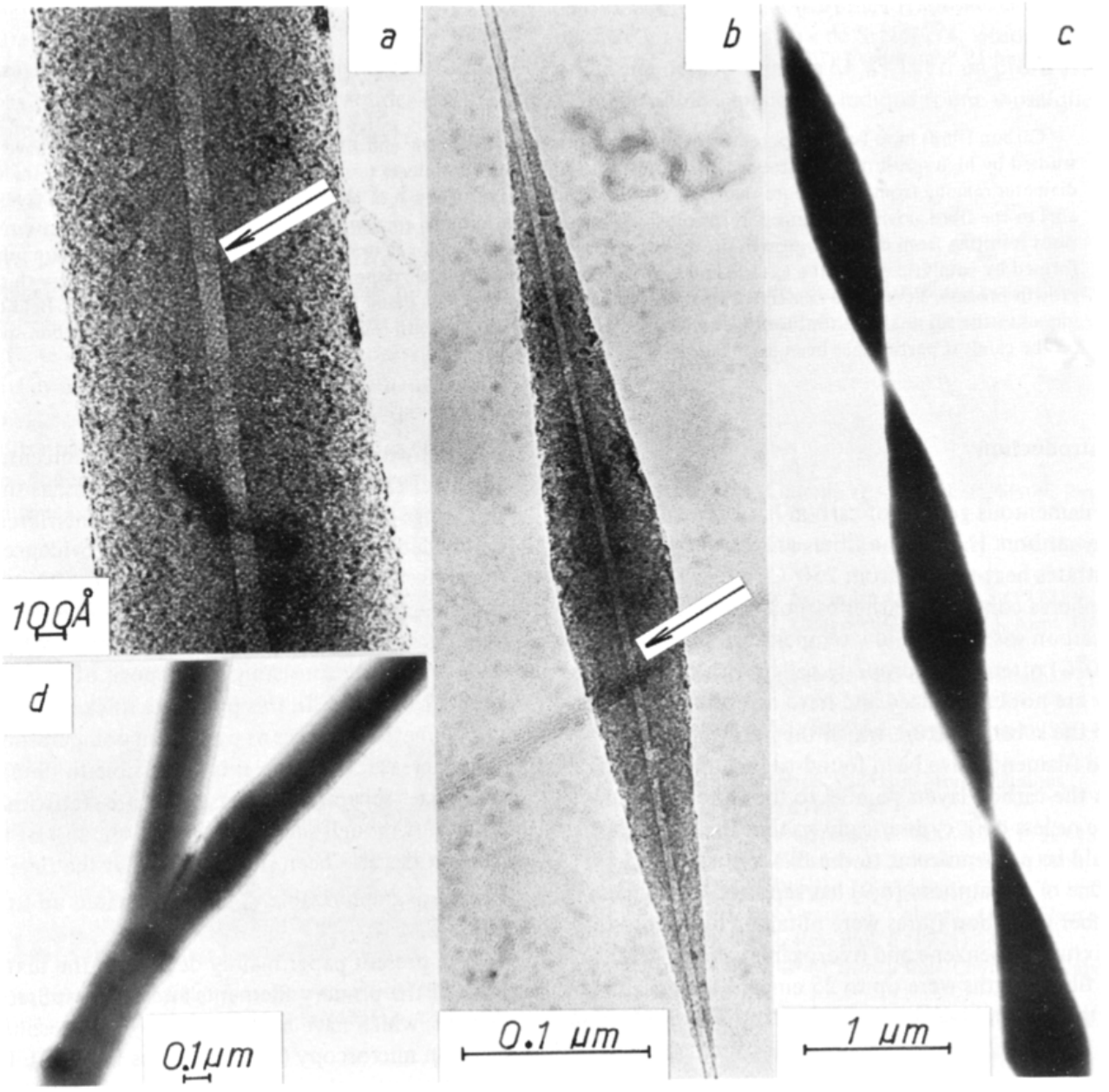

Fig. 1. Bright-field pictures of carbon fibres: (a) cylindrical, (b) spindle-shaped, (c) constricted, (d) branched

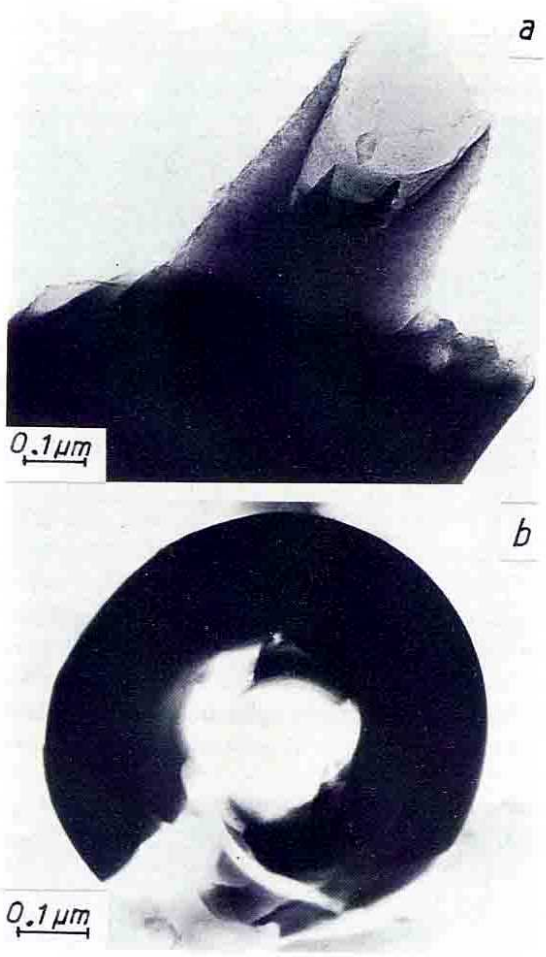

Fig. 2. (a) Fractured fibre with protruding cylindrical edge (b) transverse section (the core fell under the knife).

in fig. 1), the diameter of which widely varies from about 20 Å to more than 500 Å. The width of these tubes is not always constant over the whole length of a given fibre. The fibres are formed like a tree by concentric rings, the mutual adhesion of which is often very low. This is shown as an example in figs. 2a and 2b. In fig. 2a, the fragment of broken filament shows a large sheet peeled off while the core remains intact. In fig. 2b (transverse thin section), a part of the "annual ring structure of the tree" can only be seen; the central core fell under the microtome knife action. The core of the fibre seems to exhibit a higher strength than the outer part as shown in fig. 3.

The SAD patterns correspond to a turbostratic structure since they do not show any *hk.l* reflections characteristic of the three-dimentional crystalline order. They are representative patterns of a fibre in which all the carbon layers are roughly parallel to the fibre axis but in which the *a* axes are at random. The reciprocal space of such a fibre consists in 00.*l* nodes aligned along a direction perpendicular to the fibre axis (along equatorial line). The *hk* lines of turbostratic stacks generate concentric *hk* cylinders which turn around the fibre axis. If the reciprocal space is sectioned by a plane, a series of diffusion *hk* zones is obtained. They are limited internally by a circle centred on the 00.0 origin and externally by two straight lines parallel to the equatorial line. In fig. 4 the planar section schematically represents the case of a 10 cylinder only.

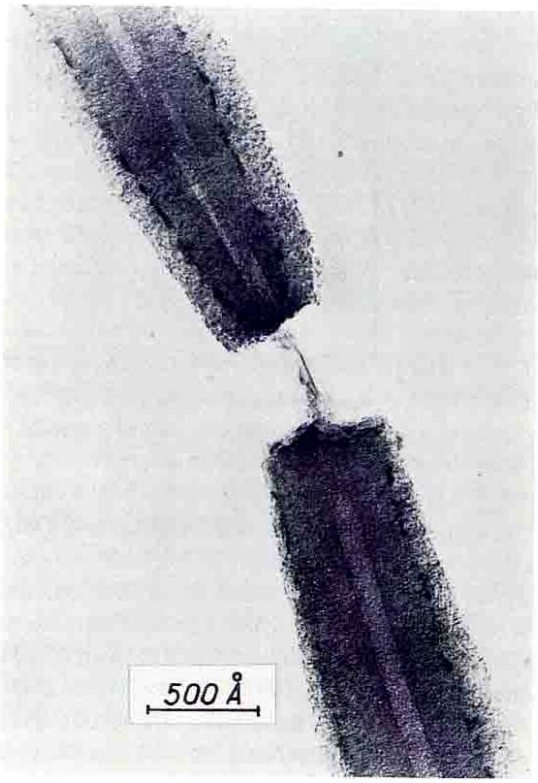

Fig. 3. Broken part of a fibre with remaining core.

When the SAD patterns are properly oriented in respect to the fibre axis (fig. 5a), they correspond to the above model. However, the 00.*l* reflections spread into arcs from 20 to 30°. The existing misorientation of aromatic layers is thus shown to be equal to this value.

These patterns cannot be used to determine wheth-

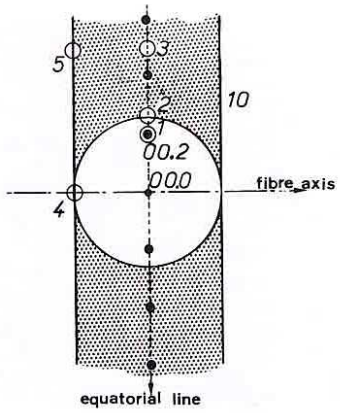

Fig. 4. Section of a part of the reciprocal space of a fibre showing various positions of the objective aperture

er the texture of the fibre is cylindrical or not. Only the dark-field technique allows such a determination. However additional information about the elementary stacks can be given by SAD patterns. First, the occurrence of high-order 00.*l* reflections (up to 00.8) indicates a good parallelism of the carbon layers as well as the absence of distorsions. Secondly, the sharpness of the 00.2 reflections depends on the diameter of the fibres. The thickest ones (fig. 5a) lead to more diffuse reflections than the thinnest ones (fig. 5b). Consequently, the number of layers per stack is smaller in

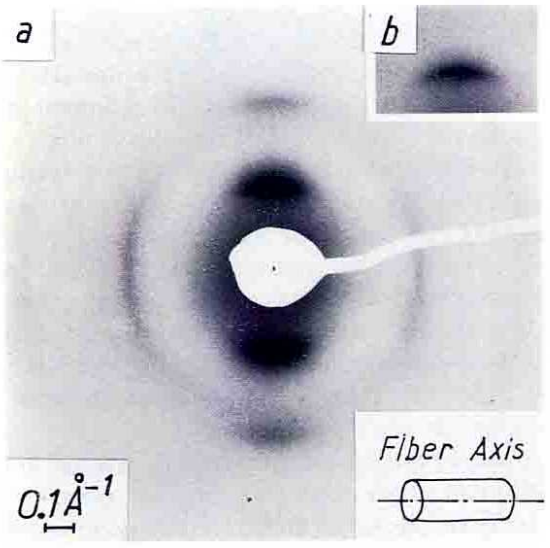

Fig. 5. Selected area electron diffraction pattern of a cylindrical fibre; the axis is perpendicular to the incident beam: (a) thick fibre, (b) thin fibre (detail of 00.2 reflection).

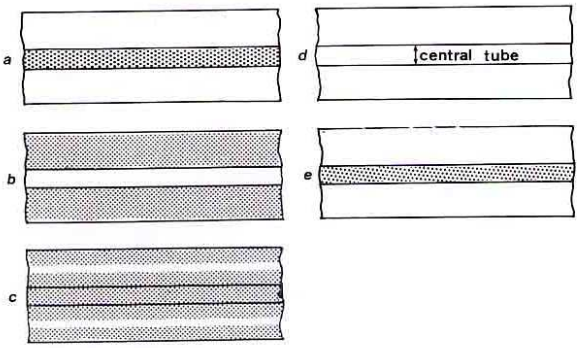

Fig. 6. Schematic representation of dark-field analysis of fig. 4.

the external parts than it is around the central core.

The cylindrical texture of the fibre can be demonstrated by dark-field analysis of the SAD pattern. Fig. 4 shows various possible positions of the aperture. The first one only intercepts the 00.2 diffracted beam. The dark-field picture becomes bright wherever aromatic layers are seen edge-on (i.e. layers parallel to the incident beam). If the texture is cylindrical, this occurs all along the fibre except right above or right below the hollow central tube (fig. 6a and 7a). The 2 posi-

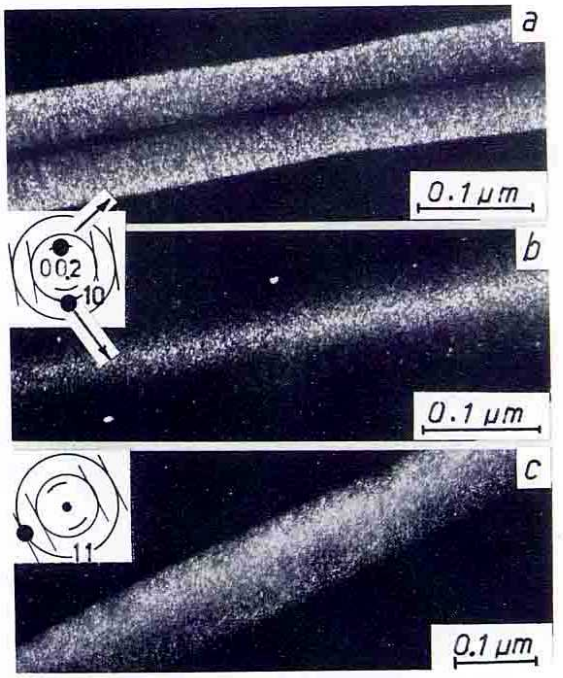

Fig. 7. Texture of a cylindrical fibre as shown by dark-field: (a) 00.2, (b) 10, (c) 11.

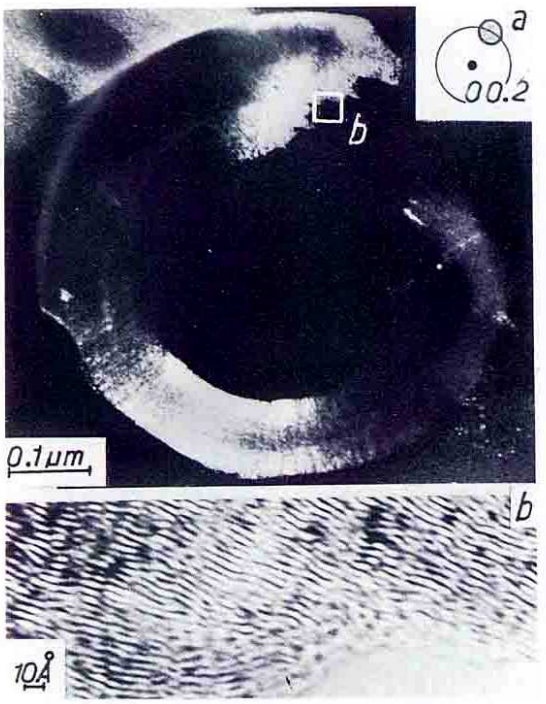

Fig. 8. Transverse thin section: (a) 00.2 dark-field, (b) 00.2 lattice-imaging of insert in (a).

tion corresponds to the reciprocal lines which are roughly parallel to the incident beam. In the optical image (figs. 6b and 7b) the central core appears as a bright band (layers seen on the upper side, i.e. normal to the incident beam). Reaching the 3 position, only the oblique reciprocal lines lead to a diffracted beam

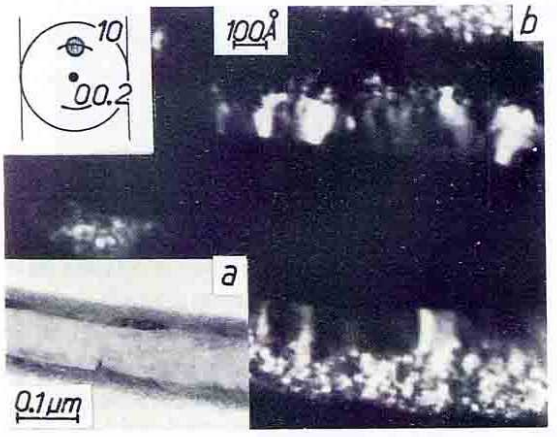

Fig. 9. Internal and external part of a fibre: (a) bright-field, (b) 00.2 dark-field.

passing through the aperture. In the image (fig. 6c) the bright central band divides into two. These two bands diverge toward the edges of the fibre as the aperture moves beyond the 3 position. On the contrary, in the 4 position, if there is no preferred orientation of the *a* axis, reciprocal lines are always found which give a beam passing through the aperture. In this case, the whole fibre appears bright (fig. 6d and 7c). Finally, in the 5 position, the aperture only intercepts the beams given by the reciprocal lines normal to the incident beam. In the image (fig. 6e) the layers seen edge-on appear bright as in the 00.2-dark-field pictures.

In fig. 8a which corresponds to a transverse thin section two bright regions only appear. It has been necessary to move the aperture 180° around the 00.2 ring in order to successively light up all the other regions of the thin section.

00.2-dark-field pictures (fig. 9b) as compared to bright-field ones (fig. 9a) show two types of regions in the fibre, suggesting a different texture. The first one lying around the central tube presents intense Bragg fringes as if it were monocrystalline. Its thickness widely varies from one fibre to another. On the contrary, the second region, corresponding to outer parts of the fibres, exhibits small bright domains well separated from each other. In order to measure their sizes, is has been necessary to use an objective aperture large enough to give in the optical image plane negligible diffraction effects. Among apertures of various diameter a 0.34 $Å^{-1}$ one has been chosen which corresponds to a 3.5 Å Airy disc [the Airy disc diameter is the width at half-maximum of the central diffraction peak given by an aperture; the diameter of this aperture is expressed in the reciprocal space from the formula $(2(\sin\theta)/\lambda)$ $Å^{-1}$]. In that case, the average size of a small bright domain is less than 10 Å. These dimensions would be expected for layers of less than 10 aromatic rings piled up by 2 to 3.

The difference between the core and the external part of the fibres as well as their concentric texture are largely confirmed by two beams lattice-imaging using tilted illumination. Fig. 8b which represents an enlarged part of the transverse thin section pictured in fig. 8a, shows that the carbon layers lie parallel to the external surface of the fibre. Fig. 10a which represents a view along the fibre axis, also demonstrates the concentric texture both through the resolution of the 00.2 fringes (corresponding to the interlayer spacing seen in

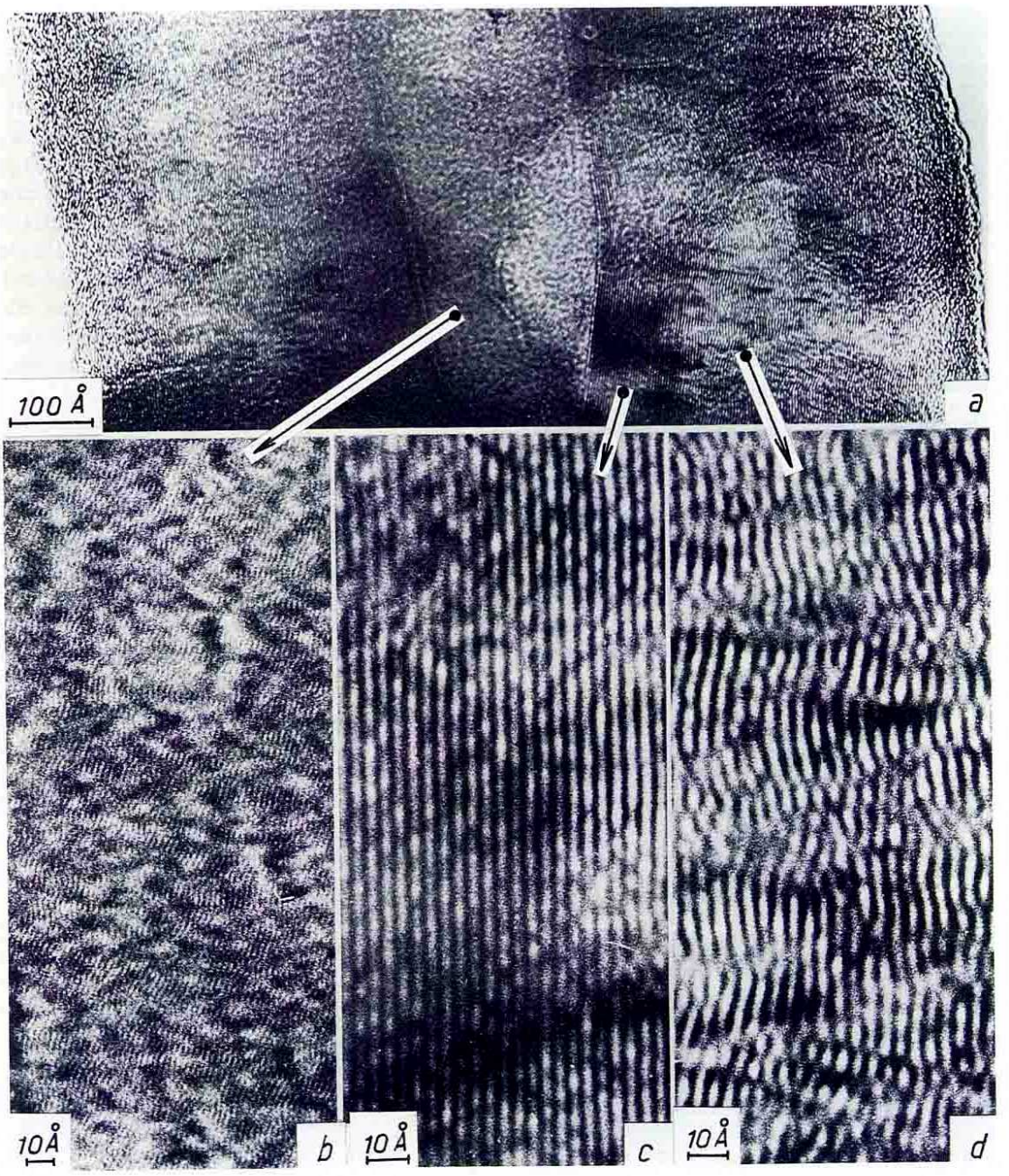

Fig. 10. Lattice-imaging: (a) view along the fibre axis, (b) 10 fringes, (c) 00.2 fringes near the hollow tube, (d) fringes in the external part

figs. 10c and 10d) and through the resolution of 10 fringes (roughly corresponding to a 2 Å periodicity seen in fig. 10b). As seen on this figure, the 10 fringes run roughly parallel to the fibre axis, in very small domains (<10 Å) separated from each other by regions out of contrast. These regions represent the portions of the fibre where 10 beams are produced which may interfere with the incident beam. This does not obviously correspond to lattice planes projection because of the turbostratic structure, but to lattice rows of

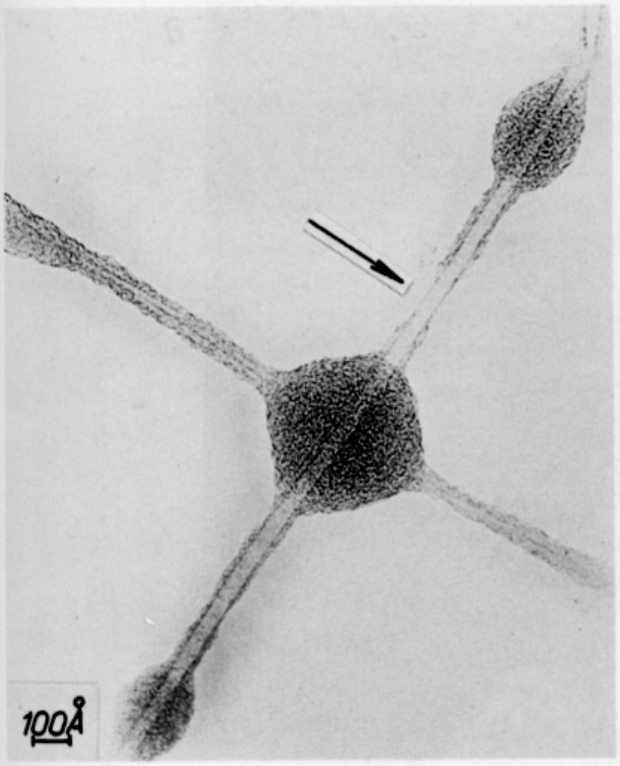

Fig. 11. Bright-field image of branched inhomogeneous fibres.

carbon atoms in a single carbon layer. Fig. 10c also shows that, near the hollow tube, the 00.2 fringes, i.e. the carbon layers, are very long, straight and perfectly parallel. The parallelism of the layers is so perfect in the vicinity of the tube that they always seem to form only one stack, thus explaining the 00.2 Bragg fringe production (which is not necessarily related to any three-dimensional order but only due to the perfect parallelism of the layers). The length of the fringes is usually more than 1000 Å. On the contrary, fig. 10d corresponding to the external part of the fibre only shows short fringes (less than 10 Å) piled up by two or three. The misorientation of one stack relatively to its neighbour ranges from 20 to 30°. This value satisfactorily agrees with the results deduced from SAD patterns. Sizes of the carbon layer stacks obtained from fringes are also in good agreement with those deduced from dark-field pictures.

The above results strongly support the occurrence of two growth processes. The first one is responsible for the formation of the inner core containing long, straight and parallel carbon layers cylindrically rolled around a hollow tube. The secondary process is the thickening of the fibre by a pyrolytic deposit. Some

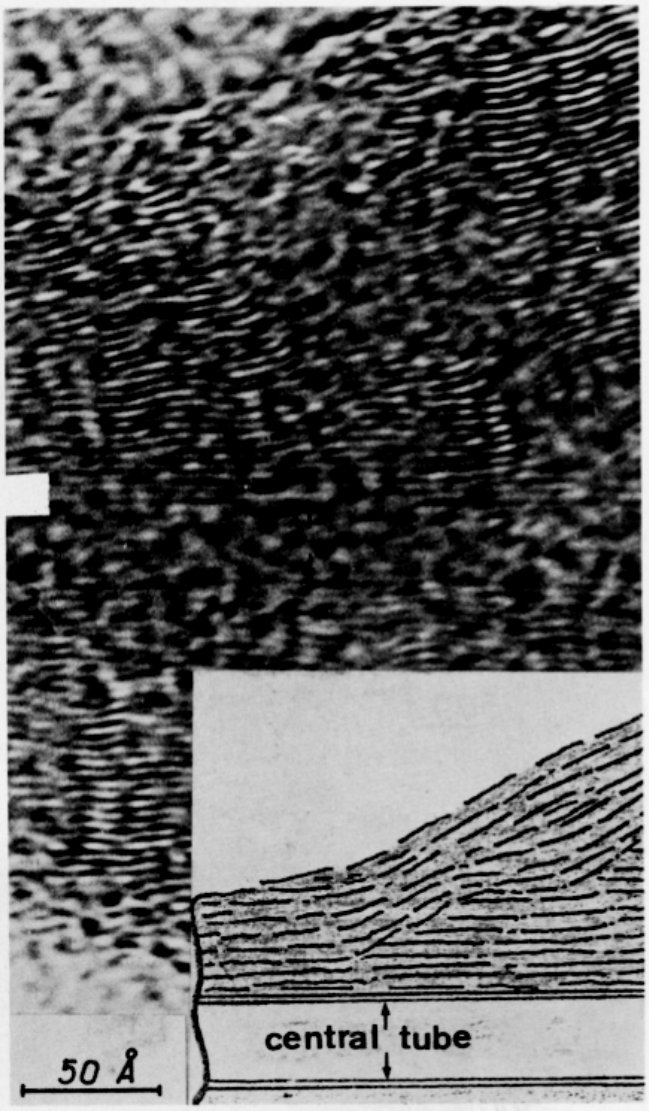

Fig. 12. (a) 00.2 lattice fringes of a constricted fibre, (b) schematic drawing of (a).

examples may be found where the internal core is only present in some part of a given fibre (see arrow in fig. 11). The same figure shows that some secondary deposit has been formed from place to place. This fact explains the conical shape of some fibres (see fig. 1c) which is probably due to an additional continuous pyrolytic deposit on an ancient one, similar to the one pictured in fig. 11. This mechanism is illustrated by lattice-imaging in the case of figs. 12a and 12b.

2.2. Tip of the fibres

Most of the fibre extremities are broken, but some of them are naturally terminated. In this latter case,

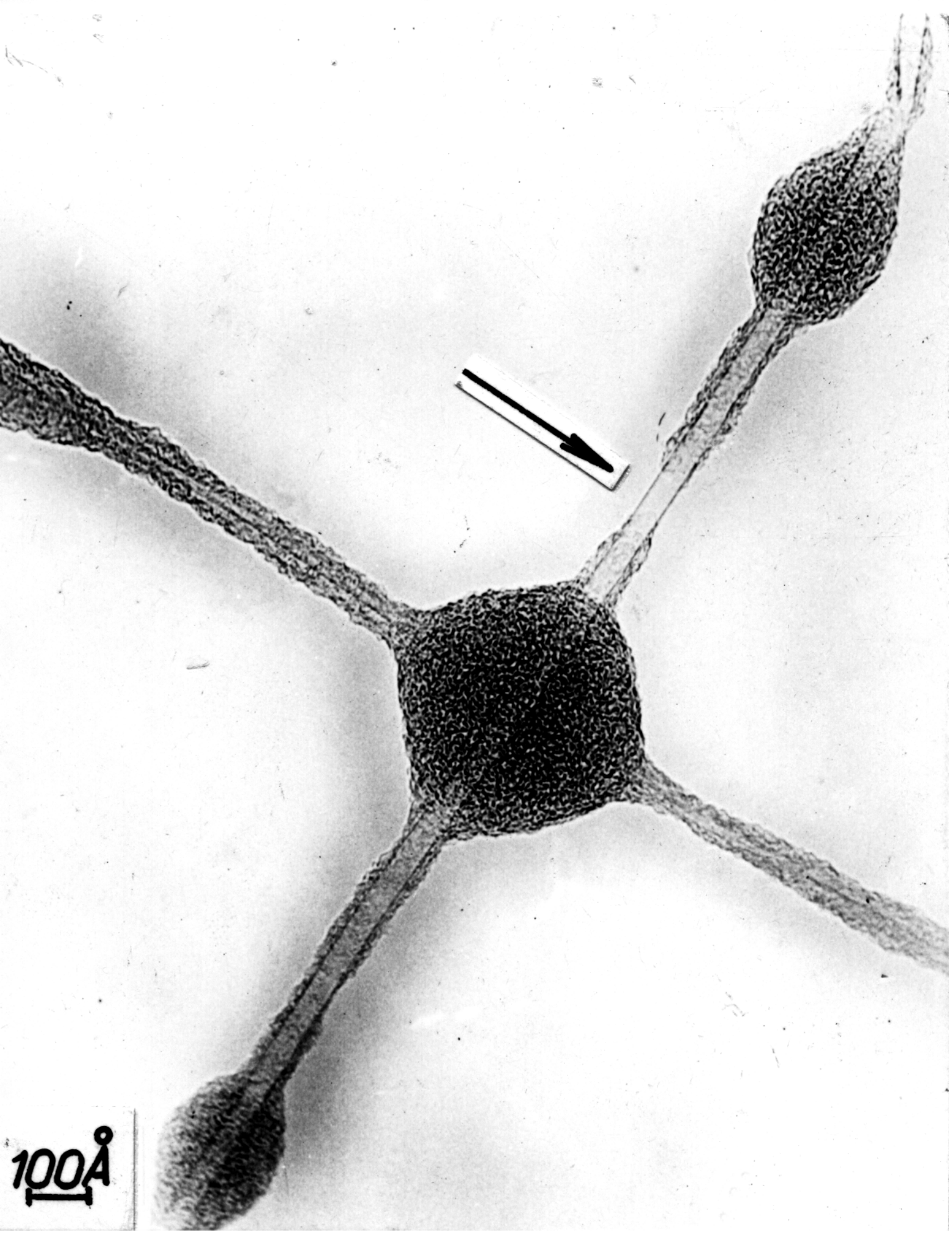
100Å

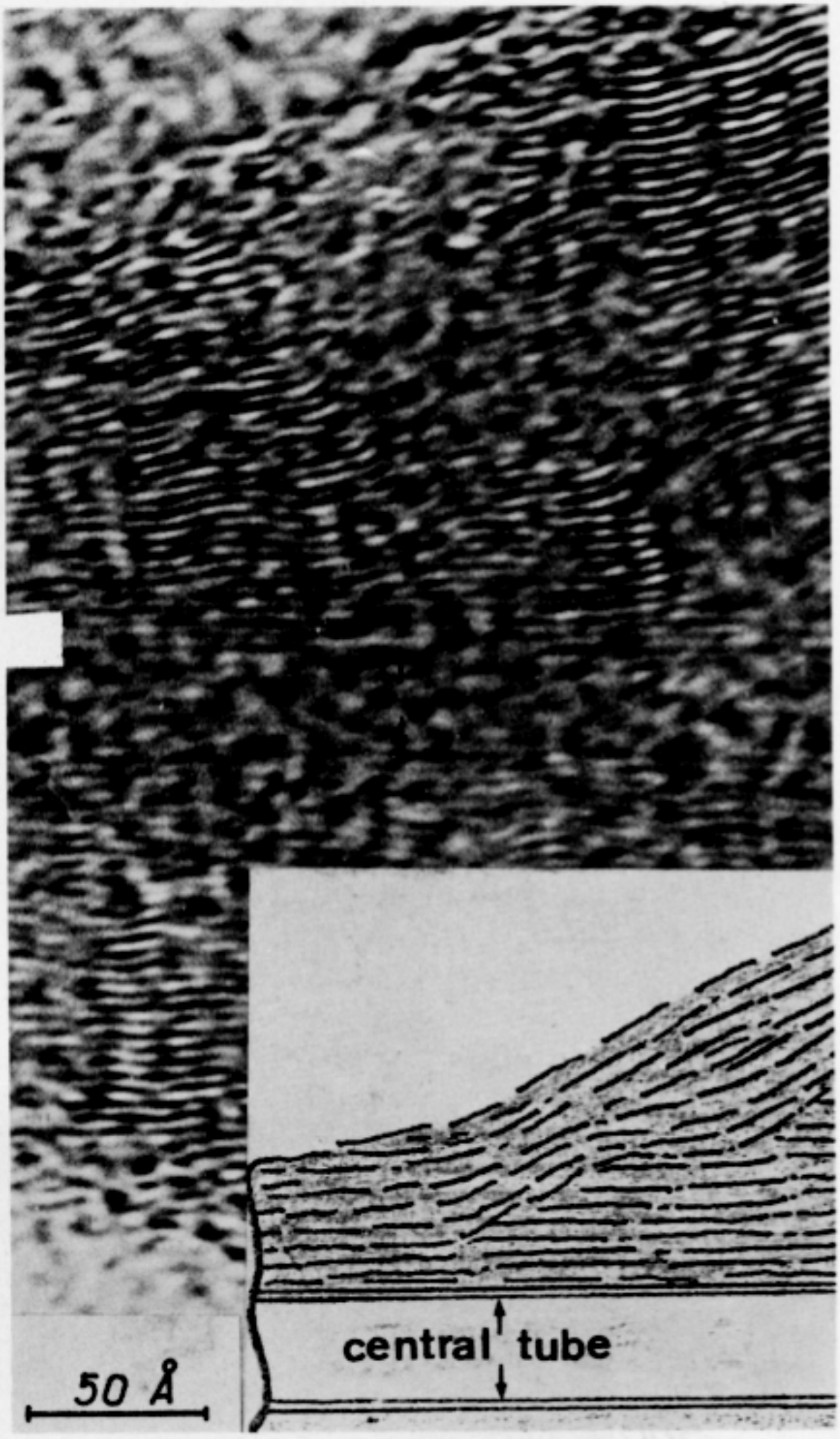

Fig. 12. (a) 00.2 lattice fringes of a constricted fibre, (b) schematic drawing of (a).

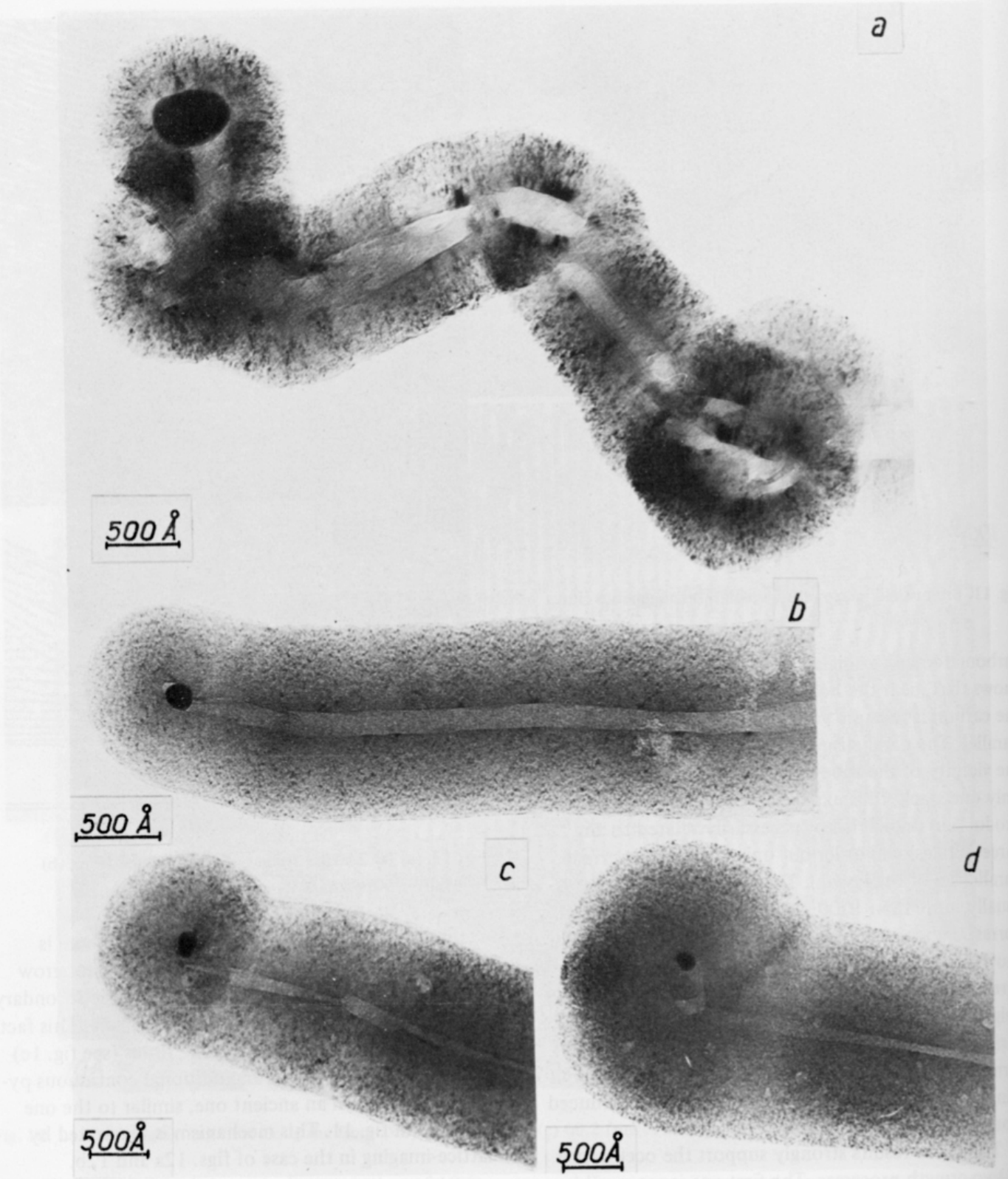

Fig. 13. Bright-field images of fibre tips showing catalyst particles.

whatever the size and shape of the fibres are, each of them contains at its tip a very small particle opaque to electrons (fig. 13). The size of these particles widely varies as it can be seen in the figure; it ranges

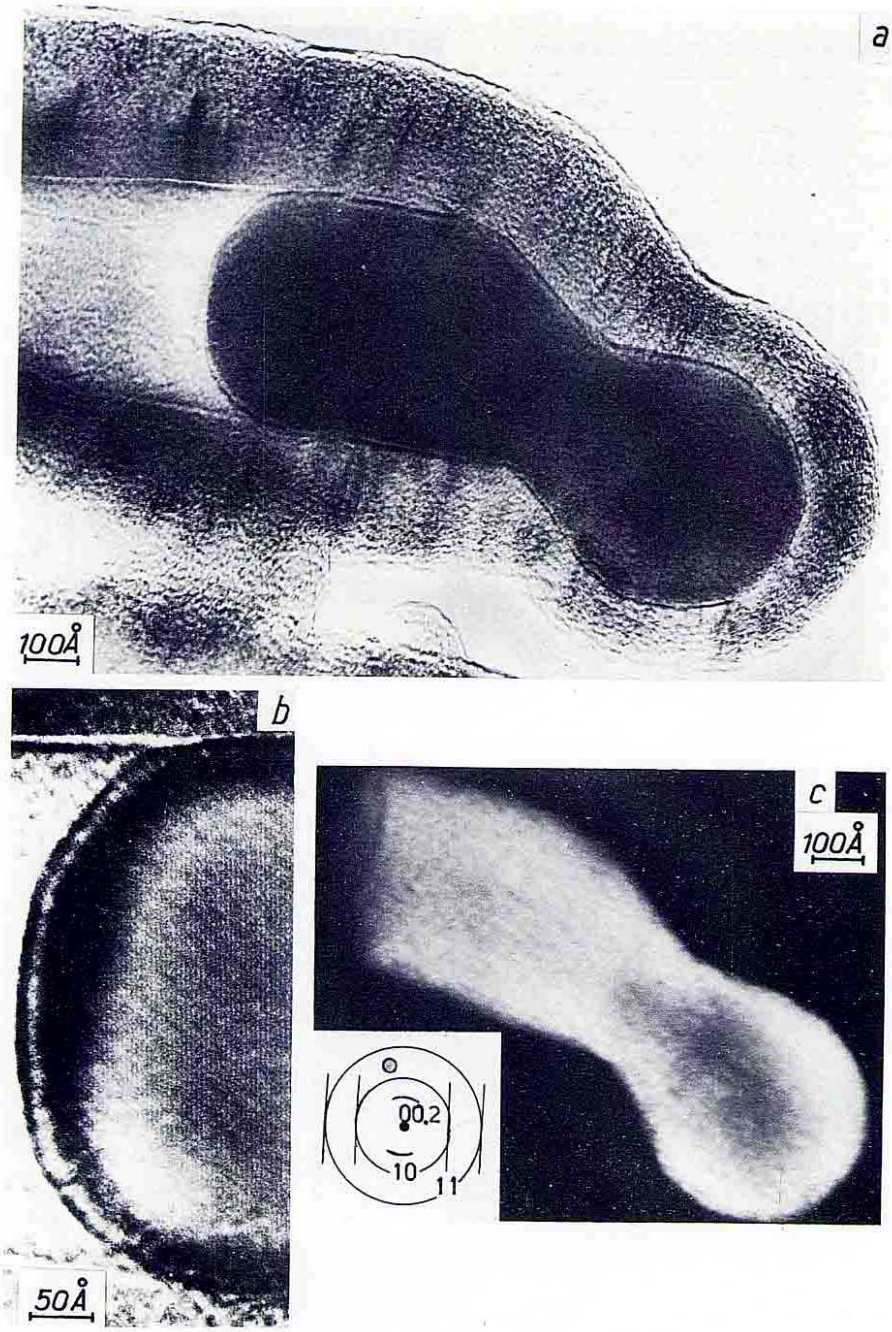

Fig. 14. Fibre tip showing FeC crystal: (a) bright-field, (b) 3.4 Å lattice fringe spacings, (c) dark-field picture with aperture centred on 210 carbide reflection (d = 1.65 Å).

from about 80 Å to 700 Å. The largest particles produce one or two very faint reflections visible in their SAD patterns. Values of d spacings thus measured suggest the possibility of either α iron or cementite Fe_3C, the most intense reflections of which being at the same place, i.e. 2.02 Å (see table 1). Lattice imag-

Table 1
X-ray powder diffraction data for Fe_3C, FeC and α-iron

Fe_3C		FeC		α-Fe	
d (Å)	*hkl*	*d* (Å)	*hkl*	*d* (Å)	*hkl*
		3.40	002		
		2.85	(102)		
		2.64	–		
		2.58			
2.54	020				
		2.50	(010)		
2.38	112, 021				
2.26	200				
2.20	120				
		2.16	110		
2.10	121				
2.06	210	2.06	111		
2.02	022			2.02	110
2.01	103				
1.97	211				
		1.93	–		
1.87	113				
1.85	122				
		1.82	202		
1.76	212				
		1.70	004		
1.68	004, 023				
		1.65	(210)		
1.61	221				
		1.56	203		
1.58	130				
				1.43	200
				1.17	211
				1.01	220

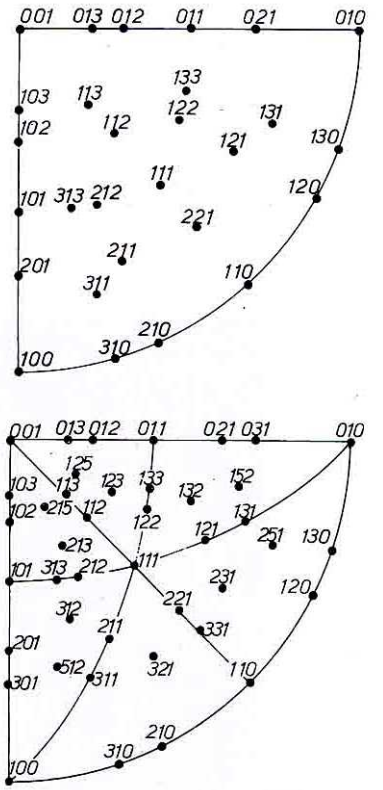

Fig. 16. Stereographic projections: (a) of Fe_3C, (b) of a cubic crystal on their (001) crystal face.

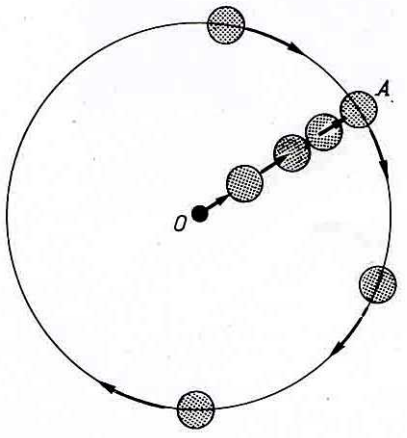

Fig. 15. Schematic representation of various positions of the objective aperture relatively to the pattern.

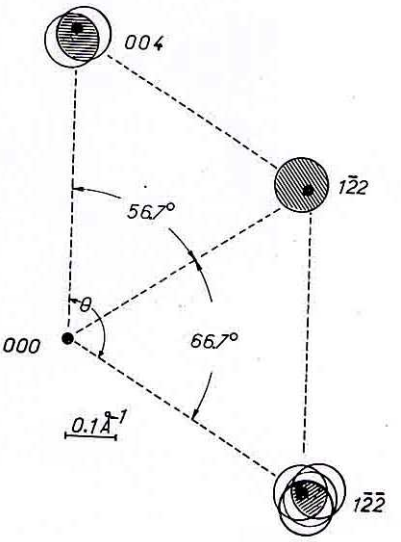

Fig. 17. Synthetic SAD pattern of small catalyst particle obtained through various objective aperture centre positions.

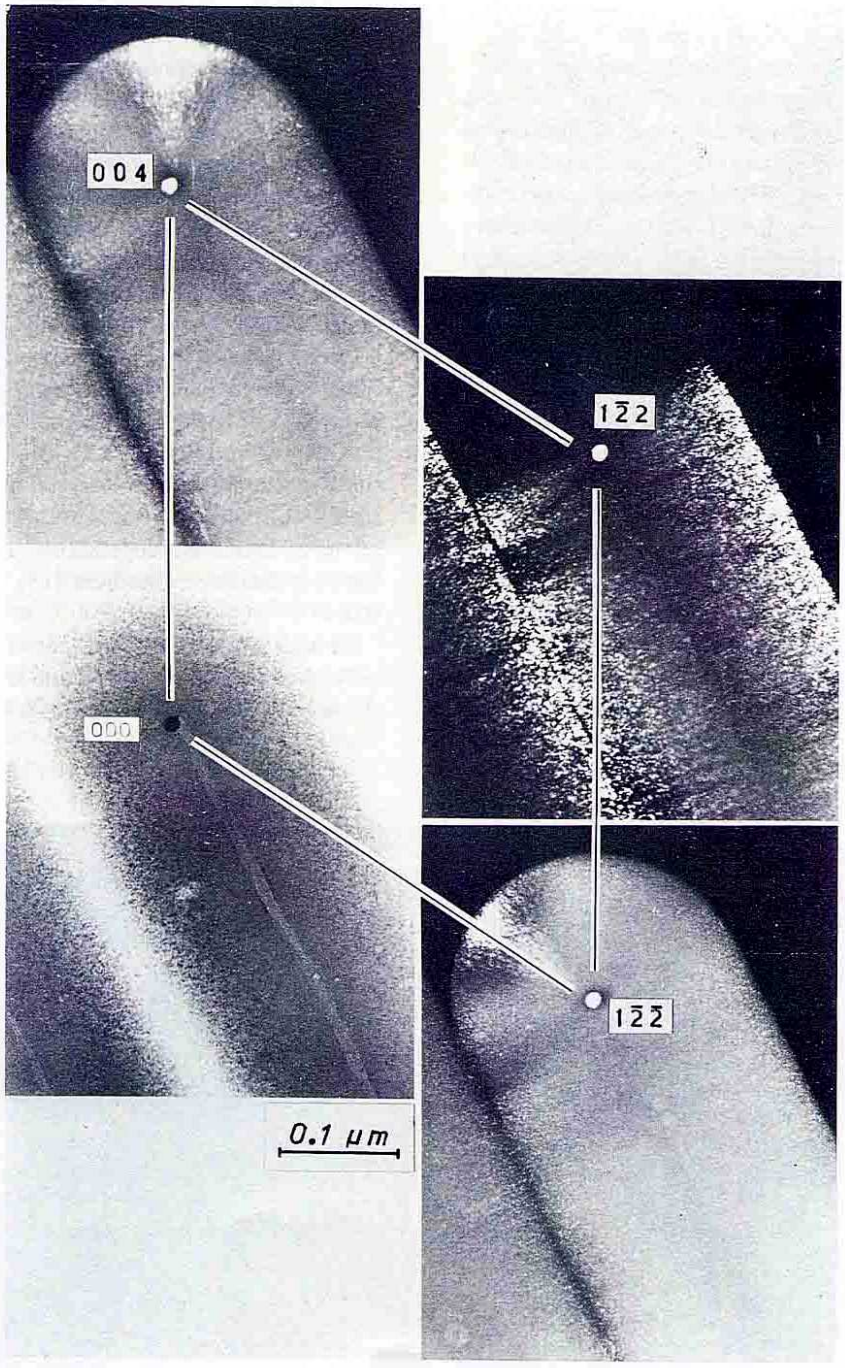

Fig. 18. Bright- and dark-field pictures of cementite crystal obtained from the fig. 17 positions of the objective aperture (the aperture also intercepts the 00.4 beam of carbon, which thus lights up).

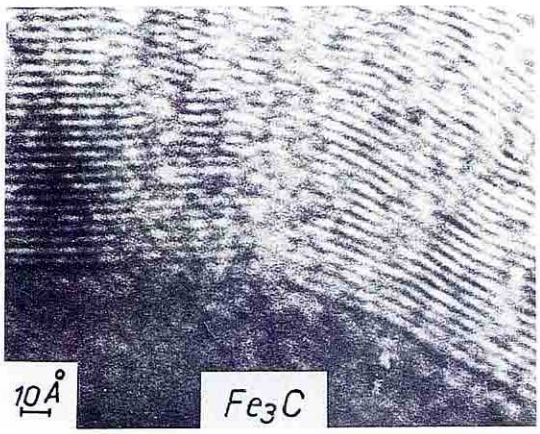

Fig. 19. Lattice-imaging of carbon encapsulating cementite crystal.

ing sometimes shows in the opaque particles, fringes with about 3.4 Å spacing eventually belonging to FeC (figs. 14a and 14b). Occurrence of iron is also suggested by spectroscopic analysis of the fibres (0.005 wt% iron content). As the smallest (and more numerous) particles are too small to give a diffraction pattern we used dark-field techniques in order to identify them.

In a previous paper, one of us has shown [13] that it is possible to measure the d spacing of a crystal as follows. A very small aperture (0.06 $Å^{-1}$) was used and the pattern was progressively tilted either radially or around a circle as indicated in fig. 15. Whenever the unknown crystal lights up very strongly in the optical image, the aperture intercepts one of its diffracted beam. Even if this latter is invisible in the SAD pattern, it can be revealed by the aperture centre position. When the crystal is lit up at its maximum, the relative position A of the aperture is pictured relatively to the unscattered beam O (fig. 15). The value of OA gives the d spacing value of the crystal if, at the same time, the $L\lambda$ constant of the apparatus is measured. Precision of the measurement depends on the aperture size and has been discussed elsewhere [13]. It is about 0.018 $Å^{-1}$.

It is known that the SAD pattern of one crystal only gives two values of d_{hkl} and the angles between the reciprocal rows, i.e. the angles between the corres-

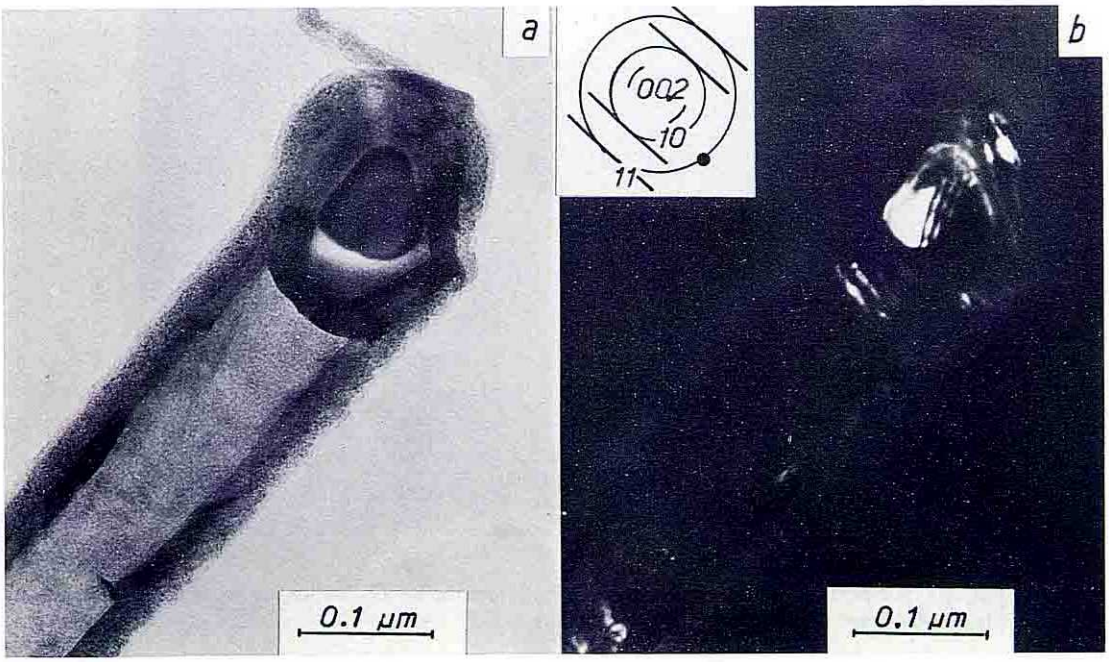

Fig. 20. Fibre tip showing relics of Fe_3C trapped within the carbon shell: (a) bright-field, (b) dark-field.

ponding planes in the crystal. Consequently, in order to identify an unknown material it is necessary to obtain more than one SAD pattern, i.e. more than one reciprocal section, and to determine the proper indices of the reflections. For that purpose, all possible crystal faces to the material have to be presented on a stereographic projection. Figs. 16a and 16b show for instance the projections for cementite and for a cubic crystal established by Andrews et al. [15]. These projections have been scaled to a Wulff pattern from which we may know all the possible angles between any reciprocal row.

Figs. 17 and 18 show an example of such a determination made on the tip of the fibre. Fig. 17 shows both the unscattered beam and every position of the objective aperture, which leads to the illumination of the small unknown particle. Some of these positions present a common part (grey areas in fig. 17). Owing to this, the location of the unknown diffracted beam becomes more precise. It may thus be deduced that the diffracted beams of the unknown particle lie on the 004 and 122 rings of cementite, and consequently do not belong to an α iron particle (see table 1). At last, the angle θ between the two reciprocal rows can be measured and its value well fits with the values calculated for Fe_3C. In fig. 18 we arranged the bright- and dark-field images in the same positions as those of the incident beam and of the diffracted beams in the synthetic SAD pattern of fig. 17. Owing to the Wulff pattern, additional information has been obtained: the indices of the crystal face which lie parallel to the supporting film; in the case of fig. 18, it is 210. The same experiments were repeated on other small particles and cementite was always found (except in the case of fig. 14c in which the position of the aperture in the pattern is compatible with FeC).

When a fibre is naturally terminated two types of carbon layer planes may occur at its tip. Sometimes the layers are long, straight and perfectly parallel to every crystalline face of the cementite crystal (fig. 19). In the other cases cementite particles are not encapsulated by a primary catalytic deposit as above, but are only covered with the secondary pyrolytic deposit. In the latter the catalytic shell narrows at its end against the carbide crystal surfaces (see fig. 14a). Relics of iron carbide layers are noticed to remain in the tip of some fibres, outside of the crystal itself but trapped in the carbon shell (fig. 20a and 20b).

3. Discussion

The above experimental results indicate that growth of thin primary fibres is due to catalytic mechanism, initiated by very small soots located in the furnace. These have been identified afterwards as iron oxide particles, reduced in pure iron by hydrogen present in the furnace. Experiments are still going on to reproduce the initial stages of growth in using small iron oxide particles.

The formation of filamentous carbon by catalytic action has been widely studied by many authors for decomposition of various kinds of hydrocarbons as well as for dismutation of carbon monoxide. Transition metals, such as iron, nickel, and cobalt, are well-known to be active catalysts, but the exact mechanism of their action is still hypothetic. Reactions are known to be favoured by presence of hydrogen, and then oxides can be used. Some authors claim that the active catalyst could be an iron carbide such as Fe_7C_3 [16], FeC [17] or Fe_3C [18]. In this case, in order to explain the hollow tube, it is necessary to assume that the carbon layers may only nucleate on a specific face of the carbide crystal. If so, a given carbide is able to solve a larger amount of poorly, than of well-organized crystalline carbon, depending on their chemical potential [18, 19]. Consequently, catalytic carbon would be produced on the active crystalline face of the carbide at the expense of the supersaturated solution of carbon contained in the carbide [20]. Such a hypothesis has the disadvantage of being based upon an hypothetic difference between the various faces of the carbide crystal. On the contrary, one of the authors [14, 21] has shown that the carbon shells resulting from carbide decomposition always present a constant thickness whatever the Miller indices of the crystal face. According to those studies, carbon layers always nucleate in a parallel direction with any available interface, only in a proportion relative to the quantity of carbon atoms provided. The interface can be either solid–gas or solid–vacuum interface [14]. Recently Baker et al. [22, 23] assume that the catalyst should be similar to a liquid droplet (which seems reasonable according to the temperature range and the size of the droplets [24, 25]). They also assume that the reaction of decomposition of the hydrocarbon, which occurs on the available portion of the droplet, is exothermic and creates a temperature gradient along the diameter of

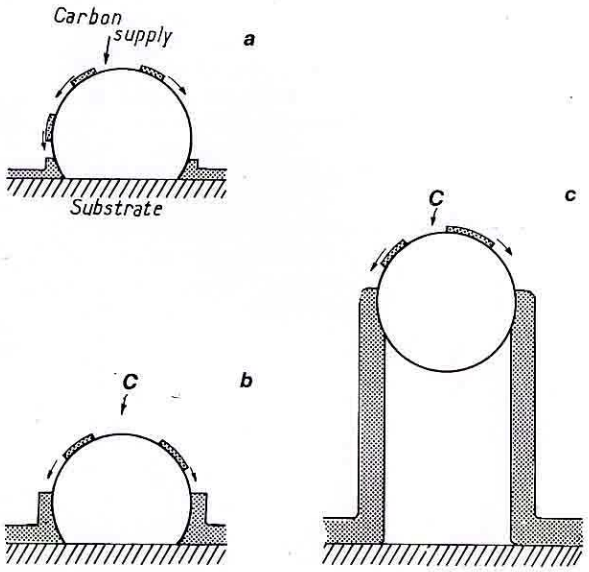

Fig. 21. Schematic illustration of fibre growth through catalytic effect.

the droplet. The carbon thus tends to nucleate on the side portions of the drop unprotected from carbon deposition because of their contact with the furnace. All these interpretations consider the diffusion of carbon atoms either through the metal or through the carbide and do not take into account any possible diffusion of metal into carbon. Moreover all of them do not really satisfactorily explain anisotropy of the growth and the occurrence of a central hollow tube.

An explanation which seems more satisfactory has been proposed by Baird et al. [26] involving a surface diffusion of "metal–metal hydrocarbon species" across the edge of the carbon layer planes. At the beginning small "liquid-like" droplets of iron get fixed on the wall of the furnace, resulting from the reduction by hydrogen of iron oxide soots. On that clean surface begins to nucleate an association of metal and hydrocarbons which diffuses on the surface and dissociates at the contact angle between the droplet and the wall of the furnace acting as a substrate. The beginning of a carbon shell is then produced. New metal hydrocarbon species dissociate on its edges and the carbon layers develop by lateral growth following the external surface of the catalyst (figs. 21a and 21b). Such a lateral growth exerts a force strong enough to lift up the catalyst particle above the surface of the substrate (fig. 21c). Layers always progress laterally in the same way and result in a filament. The hollow channel in the centre is due to the fact that no carbon supply can reach the back of the droplet, the surface of which is protected from downward surface migration by the lateral carbon layers. Growth of carbon layers would continue as long as there is a supply of metal from the top of the catalyst particle (the metal being progressively trapped between the carbon layers). When the whole droplet is covered by carbon layers at the tip, the diffusion stops and growth ends. This kind of mechanism is strongly supported by the existing relics of cementite found inside the carbon shell (see fig. 20). It must be noticed that cementite crystals are obviously formed only when cooling occurs. Such a mechanism also well explains branching of the fibres.

Increase in thickness by pyrolytic deposit on the primary thin fibres is a common phenomenon leading to graphitizable carbon. The constricted aspects often encountered at that stage of growth are probably due to the temperature gradient created along the fibre axis by a catalyst particle existing in that place. This may also be due to fluctuations of the gas flow in the reaction furnace. Anyway, such a deposit is similar to pyrolytic carbon, i.e. it is strongly oriented with its carbon layers approximately parallel to the substrate; but it is made of small turbostratic stacks with tilt and twist boundaries and thus looks more defective than the catalytic carbon contained in the core.

References

[1] W.R. Davis, R.J. Slawson and C.R. Rigby, Nature 171 (1953) 756.
[2] L.J.E. Hoffer, E. Stering and J.T. MacCartney, J. Phys. Chem. 59 (1955) 1153.
[3] L. Meyer, Z. Krist. 109 (1957) 61.
[4] M. Hillert and N. Lange, Z. Krist. 111 (1958) 24.
[5] R. Bacon, J. Appl. Phys. 31 (1960) 283.
[6] M.L. Lieberman, C.H. Hills and C.J. Miglionico, Carbon 9 (1971) 633.
[7] F.E. Wawner, Jr., J. Appl. Phys. 44 (1973) 502.
[8] T. Koyama, M. Endo and Y. Onuma, Japan. J. Appl. Phys. 11 (1972) 445.
[9] T. Koyama and M. Endo, Oyo Buturi 42 (1973) 690.
[10] T. Koyama and M. Endo, Japan. J. Appl. Phys. 13 (1974) 1175.
[11] T. Koyama, M. Endo and Y. Hishiyama, Japan. J. Appl. Phys. 13 (1974) 1933.
[12] A. Oberlin and G. Terrière, J. Microscopie 14 (1972) 1.

[13] A. Oberlin, G. Terrière and J.L. Boulmier, J. Microscopie 21 (1974) 301.
[14] A. Oberlin, G. Terrière and J.L. Boulmier, Tanso (Japan) 80 (1975) 29; 84 (1975) 16.
[15] K.W. Andrews, D.J. Dyson and S.R. Keown, in: Interpretation of Electron Diffraction Patterns (Hilger and Watts, London, 1967) p. 164.
[16] W.R. Ruston, M. Warzee, J. Hennaut and J. Waty, Carbon 7 (1969) 47.
[17] A. Oberlin and J.P. Rouchy, Carbon 9 (1971) 39.
[18] H.P. Boehm, Carbon 11 (1973) 583.
[19] J. Gillot, B. Lux, P. Cornuault and F. du Chaffaut, Ber. Deut. Keram. Ges. 45 (1968) 224.
[20] E. Fitzer and B. Kegel, Carbon 6 (1968) 433.
[21] J R. Comte-Trotet, Thesis, to be published.
[22] R.T.K. Baker, M.A. Barber, P.S. Harris, F.S. Feates and and R.J. Waite J. Catalysis 26 (1972) 51.
[23] R.T.K. Baker, P.S. Harris and R.B. Thomas, in. Proc. Intern. Congr. Carbon, Baden-Baden, 1972, p. 91.
[24] J.J. Métois, Thesis, Marseille (1974).
[25] K.L. Chopra, Thin Film Phenomena (McGraw-Hill, New York, 1969).
[26] T. Baird, J.R. Fryer and B. Grant, Carbon 12 (1974) 591.

Grow carbon fibers in the vapor phase

What you can make out of these strong materials and how to make them.

Morinobu Endo

Carbon fiber based on rayon and on polyacrylonitrile (PAN) emerged splendidly as the "Rider of the New Industrial Revolution" in the early 1960s. Today the industry has a market volume of more than 3000 tons/year and is expanding into aerospace, automobile, and construction materials applications. At the same time, users are demanding carbon fiber with diversified properties and low cost, so R&D is competing fiercely for new types of carbon fiber. The newest of these are grown in the vapor phase.

Vapor-phase-grown carbon fiber (VGCF) is generally shorter than a few decimeters; unlike PAN-based and pitch-based continuous fiber, VGCF is discontinuous. In the future, discontinuous fiber such as chopped fiber (several millimeters or shorter) and milled fiber (150 μm) will be used to substitute for asbestos and as the reinforcing agent for automobile plastics and cement. Recent demands call for carbon fiber that has unique properties in addition to strength. VGCF has a high electrical conductivity so that it can be used as filler in electromagnetic shielding plastics and other conducting materials. Such functions are inconceivable for conventional fibers.

Recent industrial research has concentrated on the use of VGCF as the discontinuous fiber for carbon fiber reinforced polymers, carbon fiber reinforced metals, and carbon fiber reinforced ceramics so that production wastes and various hydrocarbons could be used to make industrially useful materials.

The history of carbon fibers goes back to 1890 (*1*). A number of researchers had found fine fibrous carbon, quite often by accident, in carbonaceous soot and films while studying the thermal decomposition of hydrocarbons such as methane and benzene and the disproportionation of carbon monoxide. Such fibrous carbon did not attract much attention until the mid-1950s, when several important breakthroughs occurred. The proof by Herring and co-workers (*2*) that the strength of lead whiskers is close to its theoretical value excited interest in whiskers. Hillert and Lang (*3*) produced fibrous carbon (5 cm long, 200 μm in diameter) by heating nitrogen gas saturated with *n*-heptane at around 1000 °C in a quartz tube over iron or ceramic substrates. Meyer (*4*) obtained fibrous matter (1.3 mm long, 0.1 mm in diameter) by heating a carbon substrate to 2000 °C and passing over it hydrogen-diluted methane. The thermal decomposition of methane gave "carbon whiskers."

VGCFs are not single crystalline whiskers in the strict crystallographic sense; rather, the term emphasizes the engineering application of the "whiskers." Moreover, VGCFs resemble the structure and growth mechanism of single-crystal whiskers. In particular, the carbon fiber, when heated at 2800–3000 °C, is transformed from turbostratic carbon into graphite with a well-developed structure that at present is the closest to the graphite whiskers made by Bacon (*5*).

Fibrous carbon

Many of the early studies were directed toward the production and applications of such fibrous carbon but failed to determine the growth conditions and mechanisms involved, because results could not be repeated.

Figure 1 presents the two historic models proposed for carbon fiber growth: spiral growth, and a model in which carbon fiber, once formed over impurity particles on a substrate, continues to grow thereafter without any connection with impurity particles (*3*).

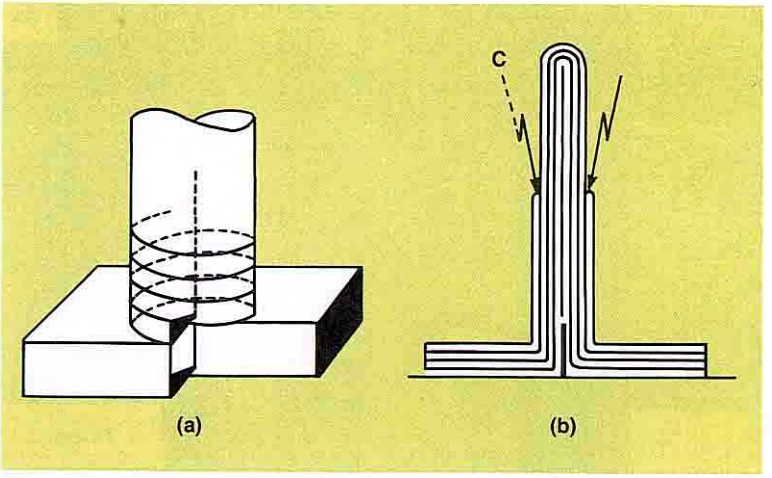

Figure 1. **Historical growth models of carbon fiber from gas phase; (a) spiral model; (b) impurity model (*3*)**

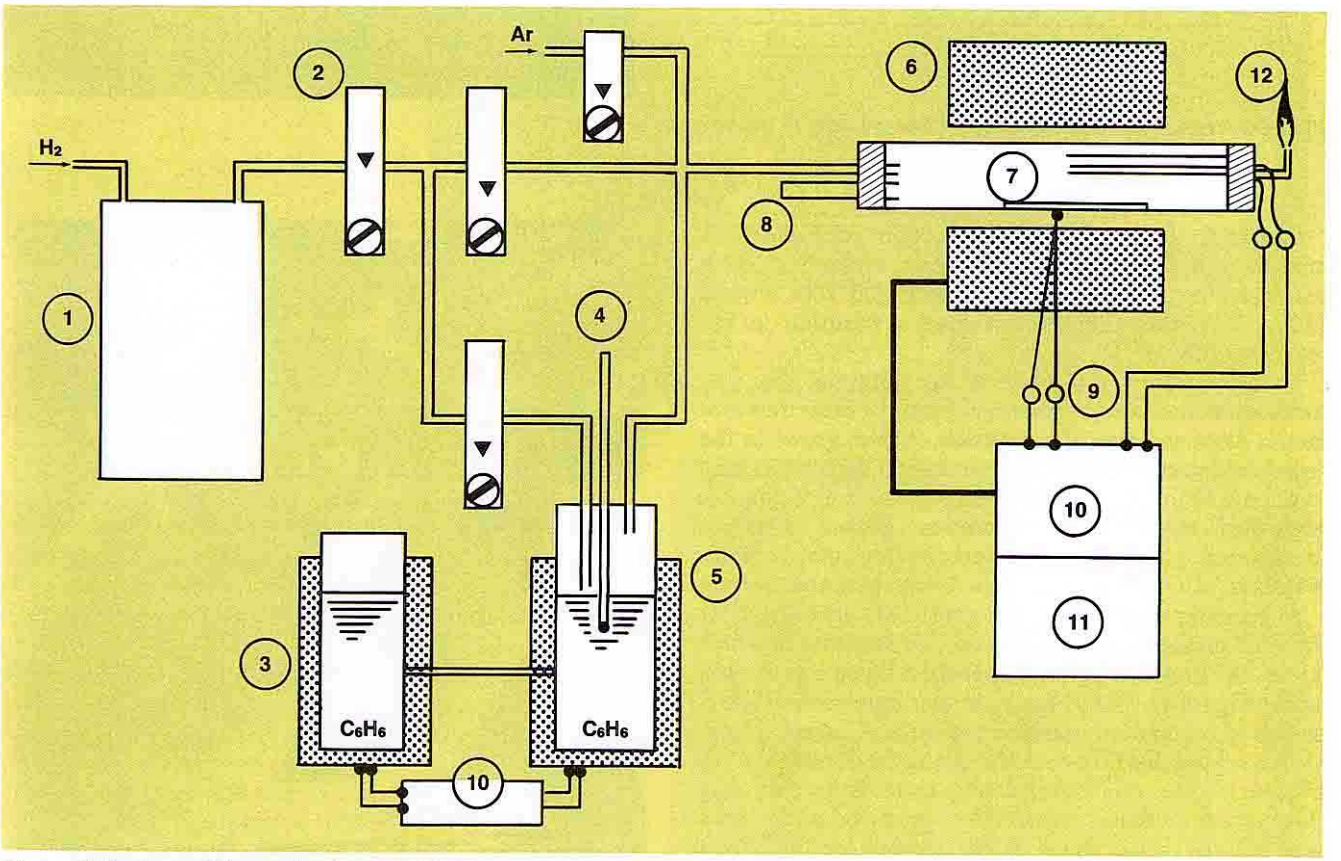

Figure 2. **Equipment for production of VGCF. 1, hydrogen purification unit; 2, flowmeter; 3 and 5, benzene; 4, thermometer; 5, thermostatic bath; 6, electrical furnace; 7, substrate; 8, observation window; 9, thermocouples; 10 and 11, temperature controller and recorder; 12, gas exhaust**

New electron microscopic analysis techniques have allowed the detailed study of these carbon fibers. Formation of mold-like or vermicular-like carbon fibers grown at 300–900 °C had been frequently reported as an abnormal phenomenon, particularly in the carbon industry. At the same time, catalyst researchers had collected detailed data relating various metallic impurities and fibrous carbon (*6*). The tiny mold-like carbon fiber, although noted as a product of interesting catalytic effects, had not been applied commercially, such as in the production of composite materials.

Carbon fiber can be made from various compounds, including benzene, hexane, allenes, and carbon monoxide. Macroscopic and microscopic characteristics of these fibrous carbon products depend on the carbon source.

We have studied schemes to mass produce carbon fibers by growing them in the vapor phase, analyzed their properties and structures, and examined applications of them. VGCF has desirable properties and is potentially competitive with PAN- and pitch-based carbon fibers (*7–9*). VGCF may be a product that "carries knowledge into a new field."

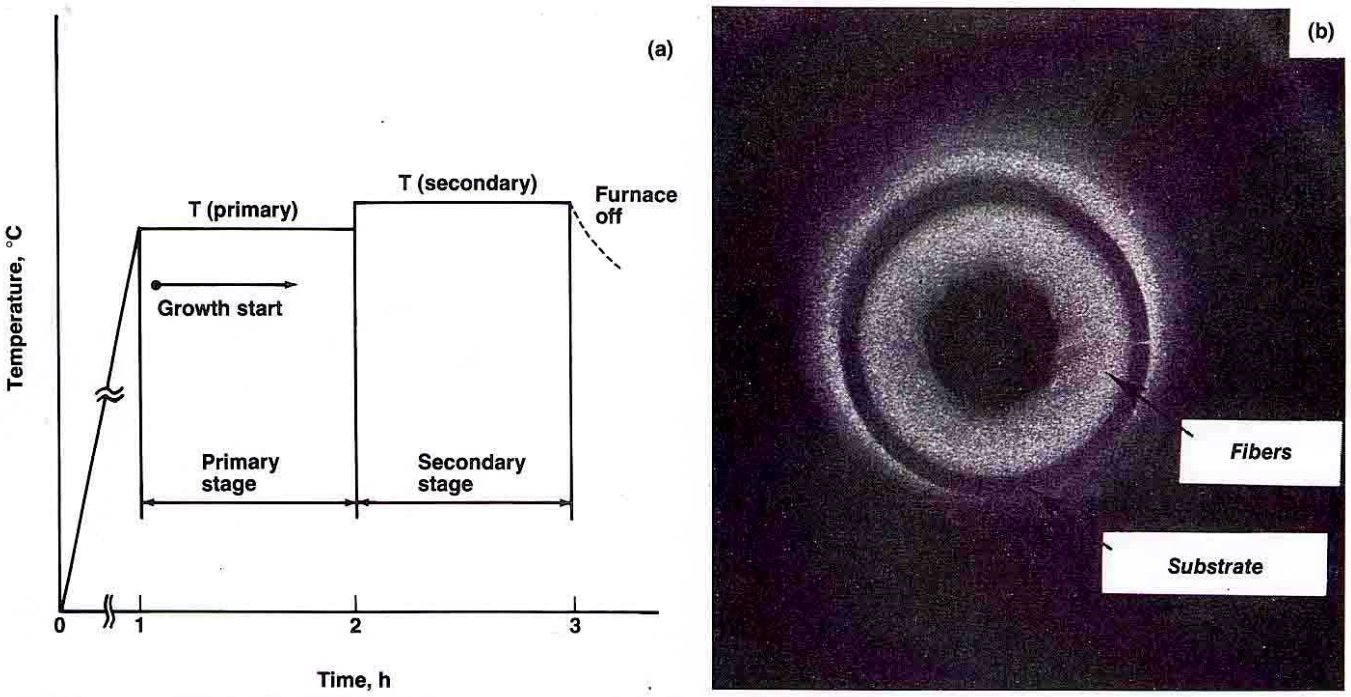

Figure 3. **Temperature program (a); fiber growing in the furnace at 1100 °C (b)**

Figure 2 depicts VGCF production equipment. A mixture of hydrogen and hydrocarbon is admitted into a reaction tube in an electrical furnace and kept around 1100 °C. Carbon fiber forms over a substrate in the reaction tube.

VGCF thus formed is grown in two steps: the fiber first forms over fine catalyst particles of iron or other relevant metals dispersed over the substrate; it then grows in the radial direction, resulting in fibers several decimeters long and about 10 μm in diameter. Temperature and timing are controlled throughout the process. Figure 3 shows temperature profiles and the fibers growing in the furnace. Note that VGCF is produced by a relatively simple system.

A scanning electron microscope (SEM) photograph of the fiber cross-section reveals a unique structure in which layers like growth rings lie concentrically on top of each other (Figure 4). VGCF has a circular cross-section and a preferred orientation in which networks of carbon planes are placed parallel to one another along the direction of the fiber axis. The orientational alignment is greater than those of conventional carbon fibers prepared in the same temperature range, which might account for the higher electrical conductivity and modulus of elasticity of VGCF.

One of the distinguishing structural features of VGCF is the presence of a hollow tube, about 10 nm or less in diameter, along the fiber axis (Figure 5a). The tube wall is composed of linearly extended, single-crystalline-like carbon layers, as shown in Figure 5c. Each layer, however, has a turbostratic stacking structure (i.e., is not a three-dimensional crystal) and does not form a three-dimensional graphite structure. The fiber periphery, on the other hand, is microcrystalline, in which two or three carbon basal networks are layered. This structure is common with thermally decomposed carbon films (Figure 5b). Thus it is apparent that the VGCF is composed of two different structures formed by different mechanisms: the catalytic growth of the fine, precursor fiber consisting of the hollow tube and linearly extended, parallel carbon layer faces near the fiber core; and the subsequent thermal decomposition of the hydrocarbons introduced by chemical vapor deposition that allows the fiber to grow in the radial direction. The physical properties of the resultant fibers are largely determined by the structures of the exterior region in thermal decomposition of hydrocarbons.

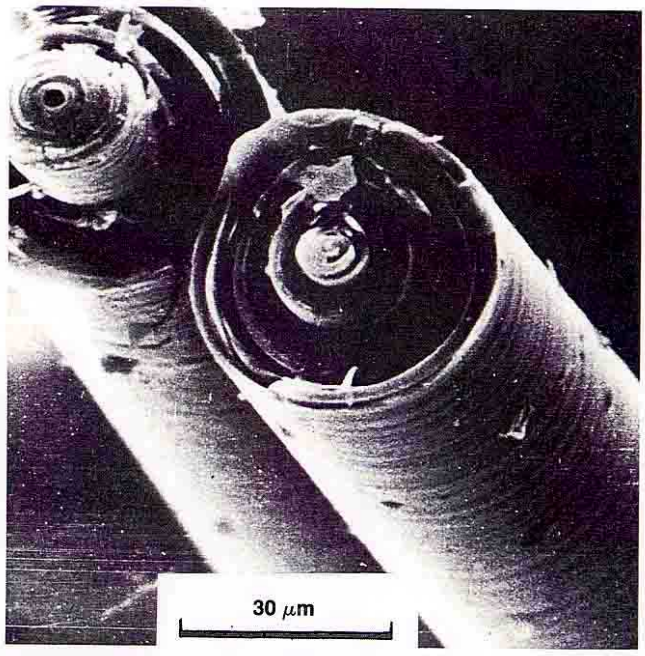

Figure 4. **SEM image of VGCF cross-section**

Mass production

The VGCF production process consists of three steps:

- seeding, in which ultrafine metallic catalyst particles serving as nuclei for the fiber growth are dispersed over the substrate surface,

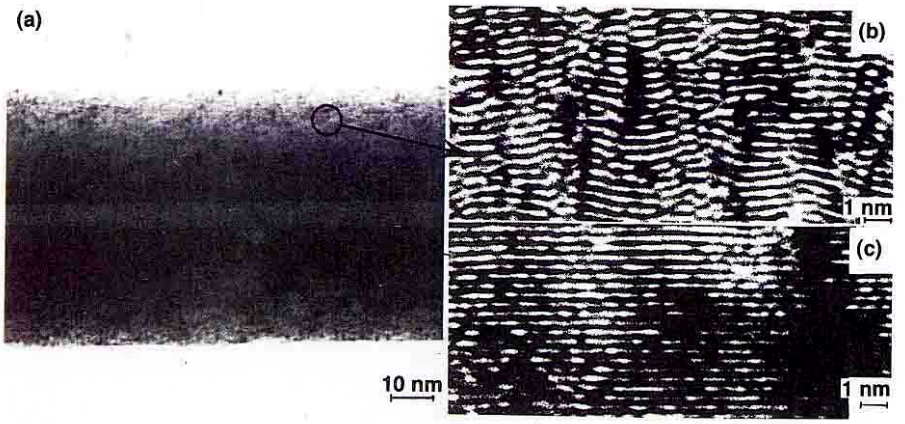

Figure 5. **Hollow tube (a) and two different structures (b, c)**

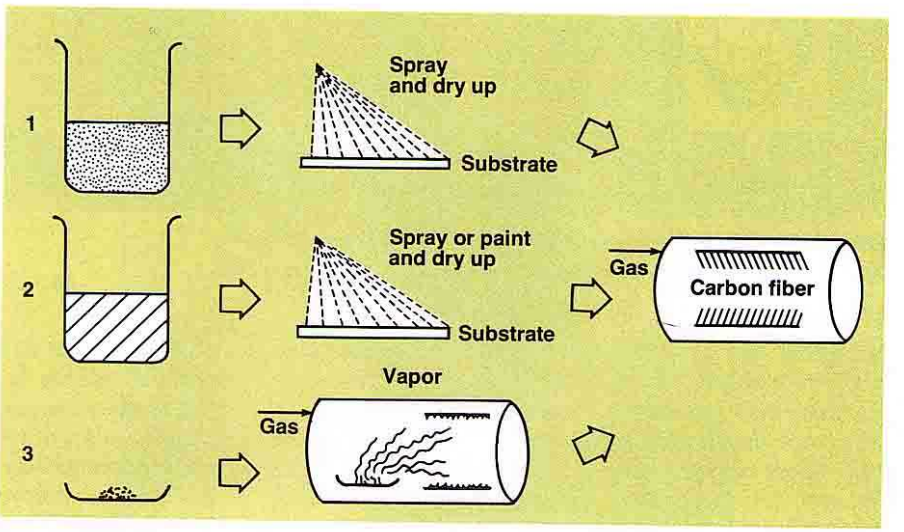

Figure 6. **Substrate seeding methods**

- growth of fine precursor fiber, and
- deposition of the thermally decomposed hydrocarbons over the precursor fiber to increase its radial size.

The dispersion of the fine catalyst particles, such as those of iron, is the key process for the mass production of VGCF. The seeding step largely determines the density of the growing fiber, i.e., the number of fibers per unit area of the substrate, and hence the productivity (7).

Figure 6 shows the three seeding approaches currently available. Approach 1 involves preparation of superfine particles of iron or other metals of 50 nm or less in size by an appropriate method such as evaporation in inert gas; the iron particles are suspended in alcohol to be sprayed and dried over a substrate. Particles having a magnetically or chemically active surface must be independently dispersed to achieve a dense growth of the fibers. Use of surfactants can promote uniform dispersion. Approach 2 attempts to spray a solution of a metal compound, such as iron nitrate, over a substrate; when heated to about 1100 °C in an electric furnace, ultrafine metal particles form. Approach 3 represents the direct seeding, in which ferrocene or other organic, metal-containing compounds are thermally decomposed and deposited over a substrate. This approach allows integration of the seeding with the subsequent fiber formation processes (9).

The seeded substrate is then heated in an electric furnace and a hydrogen–hydrocarbon mixture is passed over the substrate in a programmed process (Figure 3) to form VGCF (10 μm in diameter, 50–60 mm long). The density of the fiber formed in this manner will be about

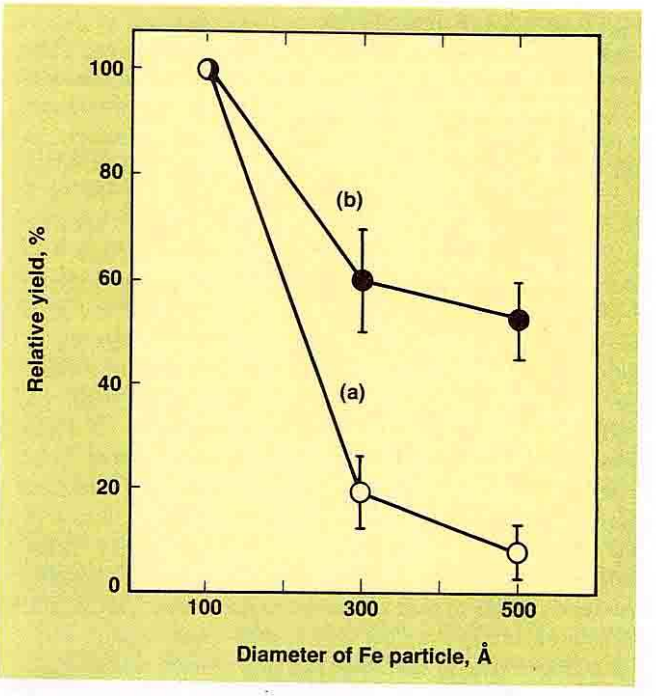

Figure 7. **Effects of catalyst particle size on VGCF yield; catalyst with narrow (a) and broad (b) size distribution**

600–1200 fibers/mm^2.

Fiber yield increases with smaller catalyst particle size (Figure 7). Growth rate of VGCF in the axial direction is 1–50 mm/min, which is 3–4 orders of magnitude higher

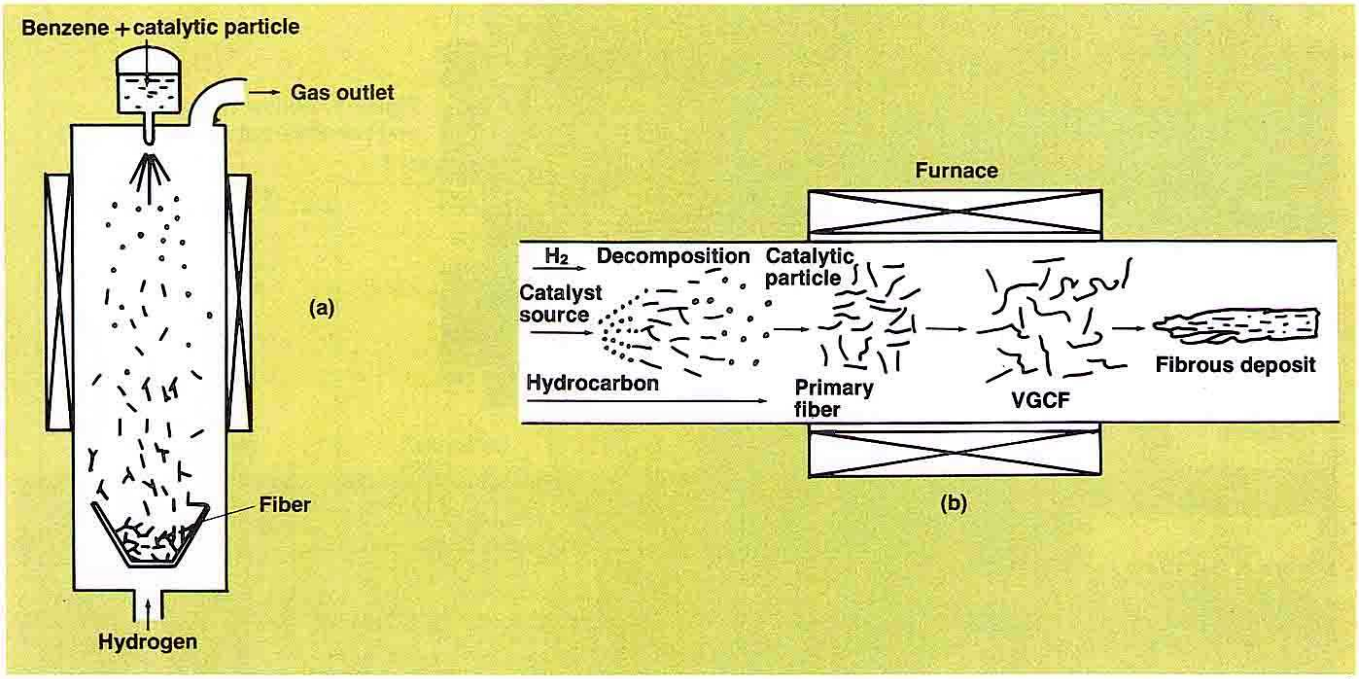

Figure 8. **Conceptual scheme of VGCF production over fluidizing catalyst particles by direct (a) and indirect (b) methods**

than those of conventional metallic or nonmetallic crystalline whiskers. This is largely due to the actions of the superfine catalyst particles.

We have developed fluidization seeding in which the initial fibers are formed over fluidized catalyst particles (Figure 8). It is much more efficient than substrate seeding for fiber formation (*9*).

Growth model and mechanism

As mentioned earlier, VGCF grows much faster than conventional whiskers, which grow at about 50 μm/s. VGCF having an aspect ratio (length/diameter) of 100 can be produced in several seconds. This ratio is equivalent to that of commercial whiskers like SiC. A reaction time of several seconds is sufficient for fine fibers to grow in a hydrocarbon atmosphere with virus-size or smaller catalyst particles. In the fluidization seeding process, the catalyst may be introduced into the reactor either directly or indirectly (Figure 8). The indirect method, by which the catalyst particles and VGCF form simultaneously, is based on Approach 3 (Figure 6). It can efficiently produce fine particles of several tens of angstroms, which, by fluidizing ultrafine metal particles introduced into the reactor in a controlled manner, greatly promotes fiber growth in the three-dimensional space of the reaction chamber. Fluidization seeding permits better control of the catalyst-feed ratio and the product aspect ratio. Fluidization-produced VGCF has a crystallographic structure similar to that of substrate-produced VGCF, but with much smaller hollow tubes of 2–3 nm (Figure 9).

It is interesting to note that the fluidization method can produce carbon fibers ranging from carbon black-like fibers with an aspect ratio of about 1 to ordinary continuous fibers, in which the aspect ratio is essentially infinite. Products having low aspect ratios can be used as reinforcing agents for various matrices, such as rubber, plastics, and cement.

Figure 10 shows the tip of a growing fiber with a crystal of iron carbide at the end of the hollow tube. The iron particle—which is either deposited on the substrate or fluidized—remains as it is while the fiber is growing but might react with the cementite particles when cooled. High-resolution transmission electron microscopy (TEM) has revealed that catalyst particles found at the fiber ends have fairly uniform sizes, mostly below 20–30 nm. Many fluidization-seeded particles are around 5 nm, which agrees with the observation that the fiber forms more efficiently with decreasing particle size. Baker and co-workers have reported that a finer particle grows the filamentous carbon faster (*10*), which may support our results for the ultrafine catalyst particles.

The fiber will continuously grow as long as the particles dispersed on the substrate or the fluidizing catalyst particles are active; the fiber ceases to grow when the particle surfaces are covered with carbon layers, oxygen, or other impurities, thus retarding movement of the carbon species. It is therefore vital to control the hydrocarbon partial pressure in the system and to keep the atmosphere free of impurities such as moisture and oxygen, in order to obtain long fibers. The TEM image (Figure 11) shows the catalyst particle at the end of the growing precursor fiber; it is not yet covered with hard, graphite-like carbon layers and can still actively assist fiber growth in the longitudinal direction. The resultant thin fibers have a continuous, thin, hollow tube as shown in Figure 11b.

We can illustrate the formation of VGCF by the model shown in Figure 12 (*11*). A reducing atmosphere of hydrogen at ~1100 °C reduces the catalyst particle of a transition metal such as iron, or cleans its surface, which promotes the polymerization and condensation of the hydrocarbon to develop hexagonal planar networks of carbon. They grow perpendicular to the substrate surface in the space between the particle and the substrate. The particle is driven upward, away from the substrate—presumably by osmotic pressure, surface tension, or

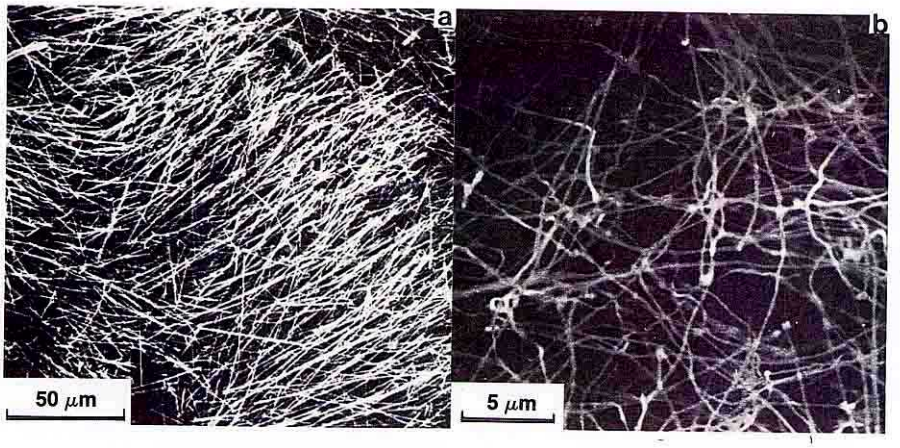

Figure 9. **VGCF produced by the fluidized seeding method; straight (a) and vermiculate (b) fibers**

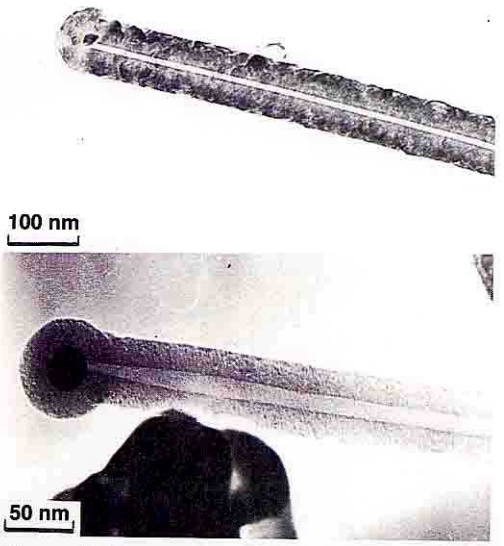

Figure 10. **Microparticle (cementite) at the tip of the hollow tube**

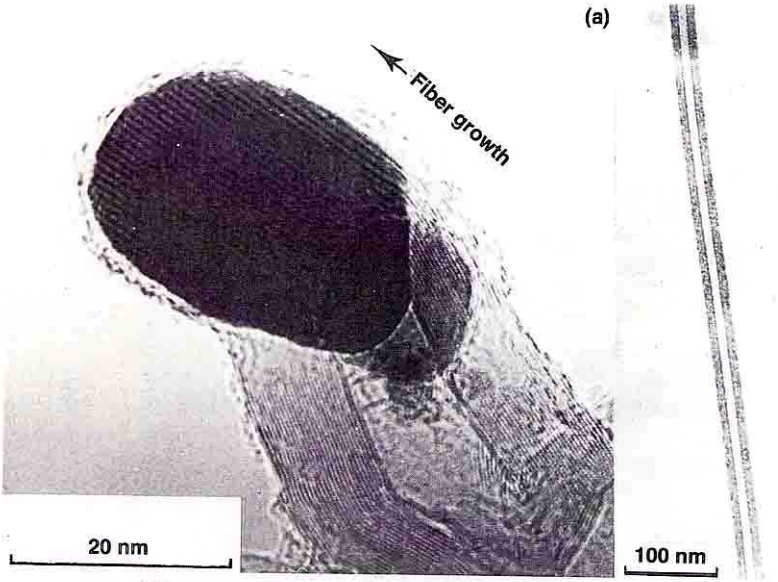

Figure 11. **Seeded microparticle at the end of the growing VGCF (a) (from a collaboration with A. Oberlin) and a thin fiber with continuous hollow tube (b)**

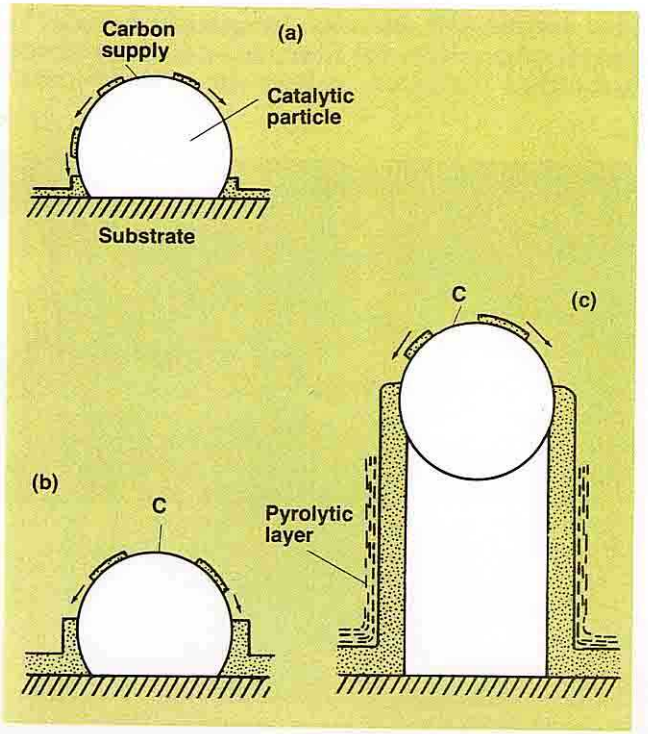

Figure 12. **Proposed growth mechanisms of VGCF (*11*)**

diffusion—and the precursor fiber formation is continued to elongate the fiber. The reactions occur in selective regions such as the surface of the catalyst particle or in some direction of the crystal. As the particle moves, it leaves behind the hollow tube. The carbon molecules within the particle move more briskly near the melting point of the catalyst, thus greatly contributing to the rapid growth of VGCF. It should be noted that the intraparticle temperature gradient provides an important force that drives the carbon species. This force, which consists of the net heat generated by the thermal decomposition of the hydrocarbon and the subsequent formation of solid carbon, promotes fiber formation. On the other hand, no fibrous carbon has been observed in net endothermic systems, such as those involving the decomposition of paraffins.

We don't yet clearly understand the extent to which intraparticle diffusion affects the overall reaction rate. Substrate seeding and fluidization seeding share common growth conditions and product structures, and, hence, growth mechanisms. If that is the case, the carbon layer plane should grow with a selective orientation for the fibrous matter to be formed over the fluidizing catalyst particles. It is therefore interesting to examine whether the catalytic effects show anisotropy. Audier (*12*) has studied

the formation of carbon fibers by the disproportionation of carbon monoxide ($2CO \rightarrow CO_2 + C$) and thermal decomposition of methane ($CH_4 \rightarrow 2H_2 + C$) over a Fe–Ni catalyst, and found that carbon is selectively absorbed on the specific crystal faces of the metal particles and separates out, after diffusing through the particles, to form fibrous carbon on the other faces (Figure 13) (*12*). The reaction temperature was fairly low (400–700 °C), and catalyst particles apparently remained solid throughout the process. It is possible that VGCF grows similarly at around 1100 °C over the solid particles.

However, we don't know yet whether each catalyst particle is in the form of a liquid droplet or a solid, nor do we know the extent to which the intraparticle temperature gradient influences VGCF formation. The net exothermic system for the formation of solid carbon from the hydrocarbon feed is also not clear, nor are the endothermic reactions involved or whether the intraparticle diffusion influences the overall reaction rate. These are some of more important questions to be solved before the growth model is fully developed.

Let me point out that the hydrogen that is used as a carrier gas plays an important role in the production of VGCF; product yield is significantly lower when nitrogen or argon is used in place of hydrogen. This means that hydrogen not only works to reduce the catalyst metal but also directly participates in the thermal decomposition of the hydrocarbons. Tesner and colleagues (*13*) reported that an acetylene-hydrogen mixture (10:90) yields ~20 times more carbon fiber than an acetylene-nitrogen mixture (10:90) over nichrome.

Industrial graphite whisker

Bacon produced graphite whiskers (2–3 cm long, 5 μm in diameter) by direct-current discharge of graphite electrodes under argon gas kept at 3900 K and 92 atm, near the triple point of graphite. For Bacon's graphite whisker, the c-axis of the crystallite crosses its fiber axis at 90°, so he proposed the structure shown in Figure 14, in which the graphite network planes are rolled into a scroll (*5*). It is not a single-crystalline whisker but can be regarded as single crystal with respect to its structure and properties along the fiber axis. It has an electrical resistivity comparable with that of single-crystal graphite. Its tensile strength of 20 GPa and modulus of elasticity of 700 GPa are the highest among those obtained so far and are close to the theoretically attainable levels of graphite. But Bacon's graphite whisker was developed under extreme conditions in very low production yield. It has not been commercially applied yet, but the work could be important to indicate the practical possible limit in strength of fibrous graphite.

VGCF is a typical graphitizing carbon; unlike pitch- and PAN-based fibers, it can be easily transformed by heat treatment into highly crystalline graphite. VGCF attains

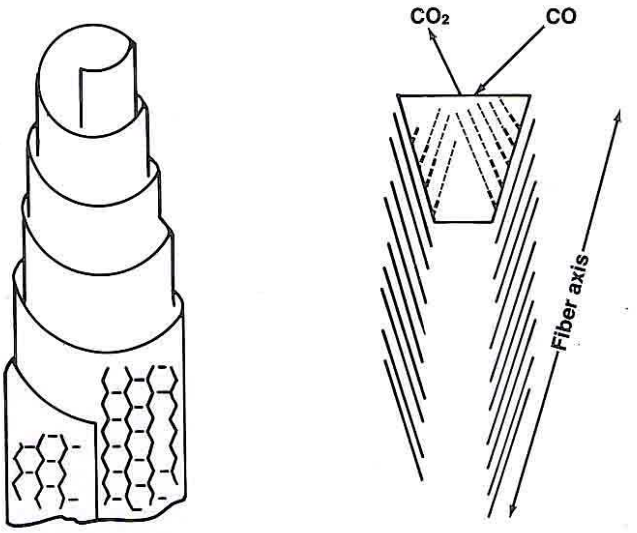

***Figure 13* (left). Growth model of hollow-tube carbon fiber grown over solid metallic particle (*12*). Note that graphite layer faces are tilting at a certain angle to the fiber axis, as if a number of cones are placed one on another, a structure that may distinguish the fiber from VGCF**

***Figure 14* (right). Graphite whisker growth model (*5*)**

an almost perfect graphite structure when heated at 3000 °C. The extent of the graphitization is higher than that of any other known fibrous carbon type. The graphite layer planes are arranged parallel to the fiber axis (Figure 15) (*14*) and can be easily produced on a commercial scale.

VGCF has desirable mechanical properties, although it is produced at the relatively low temperature of around 1100 °C. The product has almost the same properties, whether it is made from benzene or methane. Figure 16 presents the dependence of the tensile strength and modulus of elasticity of the methane-derived VGCF on fiber diameter (*15*). Its tensile strength is comparable to that of commercial carbon fibers, and it can be enhanced to as high as 7 GPa when the fiber is graphitized by heat.

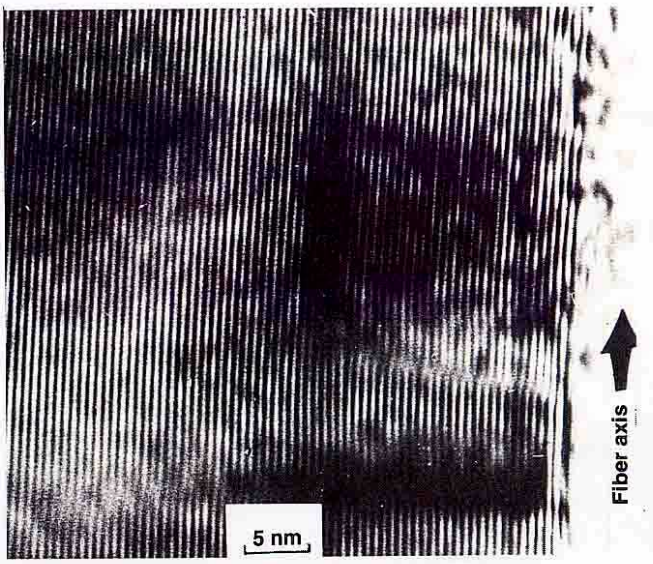

***Figure 15.* (002) lattice image of "graphite whisker" formed by treating VGCF at 2800–3000 °C**

To this point, we have worked on improving the carbon fiber's mechanical properties. More recently, however, it has become imperative for researchers to direct their efforts to imparting novel functions to the fibers so as to widen their applications. VGCF has higher electrical and thermal conductivity than any other fiber; its resistivity at room temperature is 10^3 $\mu\Omega \cdot$ cm. When it is treated at 3000 °C, its thermal conductivity at room temperature is about 4 times higher than that of copper (*16*). These properties, coupled with a high mechanical strength, will give unique properties to the composite materials it reinforces.

VGCF with rather thick diameters (10 μm) can be also used as a host material for graphite-intercalation compounds (GICs) (*17*), which can be made as conducting materials and are useful for battery electrodes. They can be used to strengthen synthetic metal wires and will have a much higher performance index (electrical conductivity/density). On the other hand, VGCF treated above 2900 °C to form graphite fiber is best suited as a host material for GICs, which have low resistivity. For example, the GIC with AsF_5 has a resistivity of 1.1–3 $\mu\Omega \cdot$ cm at room temperature and is relatively air stable. The latter GIC is thermally stable below 325 °C and is applicable to various lightweight conducting composite materials. Futhermore, we have shown that the fluorine-intercalated VGCF is suitable as an active component for anodes of high-performance lithium batteries.

Future prospects

The inherent properties and structural characteristics of VGCF will make it a suitable material for various purposes (*16*). In particular, its mechanical, electrical, and thermal

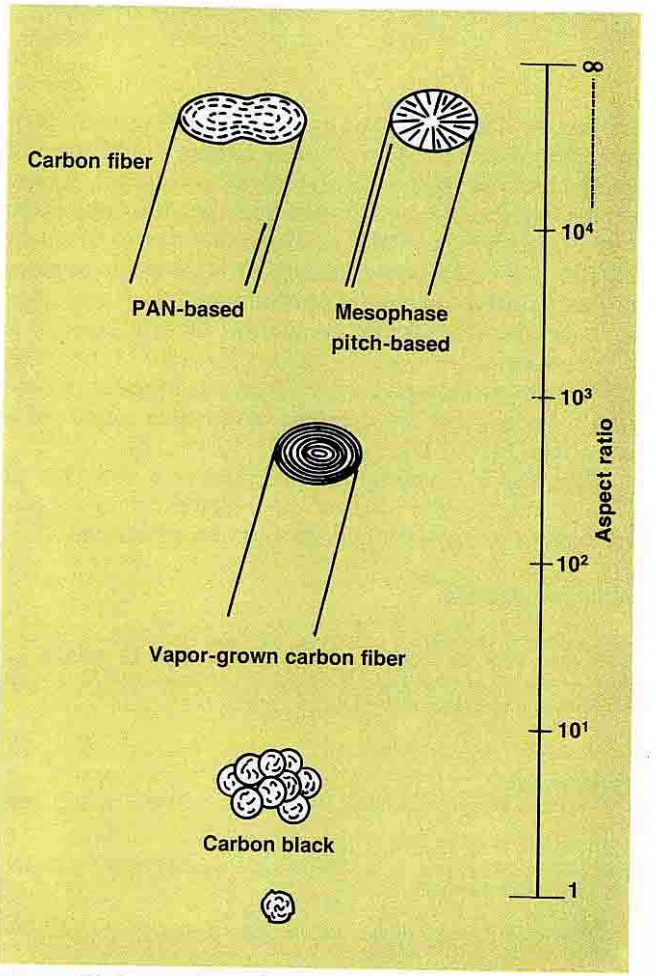

Figure 17. **Comparison of aspect ratio as a filler material for composites**

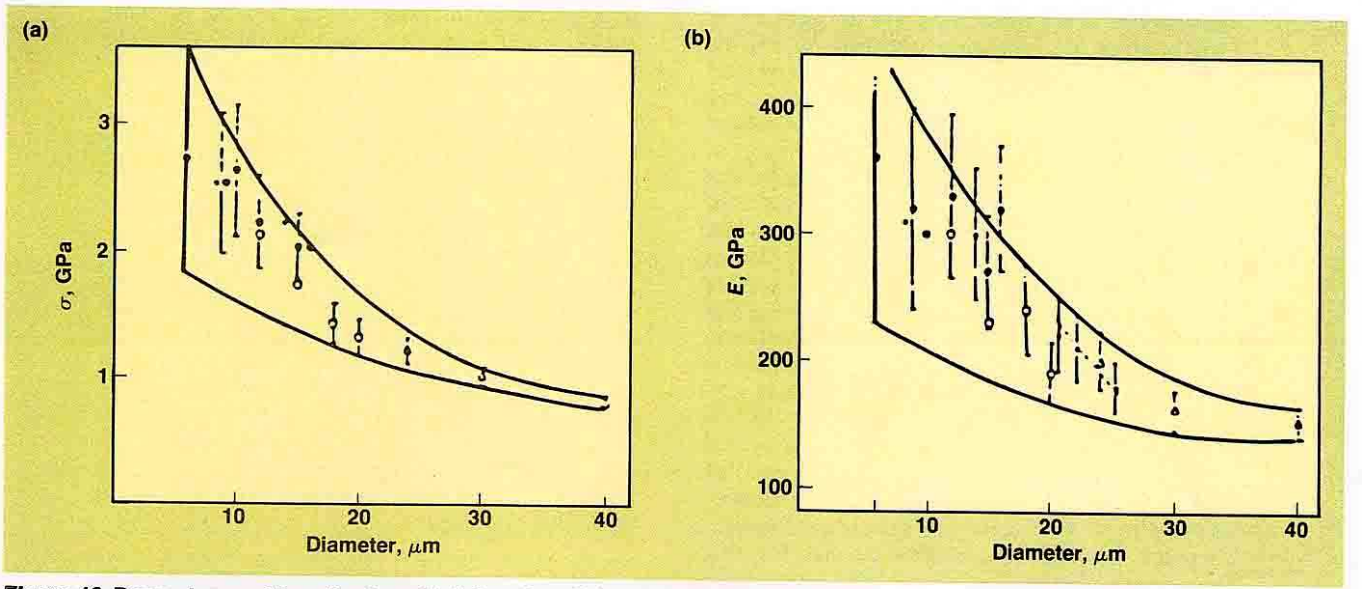

Figure 16. **Dependence of tensile strength (σ) and modulus of elasticity (E) of VGCF on fiber diameter (*15*)**

properties will further open up new application areas, such as electronics and high-tech areas related to biology and energy. Another area added recently is nuclear energy production, because VGCF has been proved to be more resistant to neutron irradiation than other carbon fibers. In addition, it could be sufficiently low-priced to replace ordinary carbon fibers in discontinuous yarn and thus serve as a useful filler for composites. In that capacity it will be located between the carbon black and continuous PAN- and pitch-based carbon fibers. Its applications are likely to expand into automobiles and construction materials (Figure 17).

Thus VGCF is emerging in markets as a new type of carbon and graphite whisker and is under extensive study for both basic research and for future applications.

Acknowledgment

The author thanks Dr. T. Koyama, Professor Emeritus of Shinshu University, Prof. M. Inagaki of Toyohashi University of Technology, Prof. A. Oberlin of CNRS, and Prof. M. S. Dresselhaus of MIT for their continuous encouragement and useful suggestion.

References

(1) Schutzenberger, P.; Schutzenberger, L. *C. R. Acad. Sci. Paris* **1890,** *111,* 774.
(2) Herring et al. *Phys. Rev.* **1952,** *85,* 1060.
(3) Hillert, M.; Lange, N. Z. *Kristallogr. Kristallgeom. Kristallphys. Kristallchem.* **1958,** *111,* 24.
(4) Meyer, L. Z. *Kristallog.* **1957,** *109,* 61.
(5) Bacon, R. *J. Appl. Phys.* **1960,** *21,* 283.
(6) Baker, R. T. K.; Harris, P. S. In *Chemistry and Physics of Carbon*; Walker, P. L., Jr.; Thrower, P. A., Eds.; Marcel Dekker: New York.
(7) Endo, M.; Komaki, K.; Koyama, T. Presented to the International Symposium on Carbon, Toyohashi, Japan, 1982.
(8) Endo, M.; Komaki, K. Presented to the 16th Biennial Conference on Carbon, University of California, 1983.
(9) Endo, M.; Shikata, M. *Oyo Buturi* **1985,** *54,* 507.
(10) Baker, R. T. K.; Harris, P. S.; Thomas, R. B.; Waite, R. J. *J. Catal.* **1973,** *30,* 86.
(11) Oberlin, A.; Endo, M.; Koyama, T. *J. Crystal Growth* **1976,** 32, 335.
(12) Audier, M.; Coulon, M. *Carbon* **1985,** *23,* 317.
(13) Tesner, P. A.; Robinovich, E. V.; Rafalkes, I. S.; Arefieva, E. F. *Carbon* **1970,** *8,* 435.
(14) Chieu, T. C.; Dresselhaus, M. S.; Endo, M. *Phys. Rev.* **1982,** *826,* 5867.
(15) Kandani, N.; Coulon, M.; Bonnetain, L. In *Extended Abstracts of Carbon '84*; Bordeaux, France, 1984; p. 142.
(16) Piraux, L.; Nysten, B.; Haquenne, A.; Issi, J. P.; Dresselhaus, M. S.; Endo, M. *Solid State Commun.* **1984,** *50,* 697.
(17) Dresselhaus, M. S.; Dresselhaus, G. *Adv. Phys.* **1981,** *30,* 136.
(18) Tibbetts, G. G.; Endo, M.; Beetz, C. P., Jr. *SAMPE J.* **1986,** *22–5,* 30.

Morinobu Endo is Professor of Shinsu University (Faculty of Engineering, Shinsu University 500, Wakasato, Nagano, 380, Japan). His current work ranges from basic science to applications on vapor-grown and mesophase pitch-based carbon fibers, graphite intercalation compounds, and silicon carbide new ceramics. After receiving a M.S. degree from Shinsu University, he obtained a Ph.D. from Nagoya University. He has worked with A. Oberlin of CNRS, France, and M. S. Dresselhaus of MIT. He is editor of the *Japanese Carbon Society Journal.*

HELP WANTED

The environment in which technical professionals must operate is far from ideal. We are confronted with hesitant and uncertain political leadership, which in turn leads to an incoherent and certainly inconsistent national science policy. The key problems addressed by politicians and government today deal with such important matters as preventing war, controlling the economy, abolishing poverty, and providing a healthful environment. It is clear to us, but not to politicians nor our government, that central to the achievement of those desires is technological progress. Many of our industries are reacting to domestic and international political and marketing problems by focusing on short-term objectives to the detriment of technological development and productivity improvement, so vital to our nation.

The opportunities for further strengthening that position abound. One way is by proposing qualified engineers for service in government—particularly this year as we look ahead to a new administration. There is a very tight time window between Election Day and selection by federal transition teams of the people who will fill cabinet posts and other positions at every level of government. ASME is now working with AAES in an effort to fill several of these positions with engineers—positions that *ought* to be filled with engineers.

We must continue to work hard to convince our members that their participation in government through testimony or through offering their expert advice is essential to the development of rational legislation.

There is an opportunity building for the ASME Council on Public Affairs to take a leadership position in advocating and contributing to the establishment of National Technological Goals. In my view, the philosophical debate that is raging on that subject is out of date. We can no longer afford to scatter our talents and resources in research and development as we have done in the past. We can no longer afford to live with the dismal performance in reducing innovation to practice. We must establish technological goals at a national level to alleviate those shortcomings.

Ernest L. Daman
President, ASME